PIBB 生物化学与生物物理进展
Progress in Biochemistry and Biophysics
2018, 45(2): 170~192
www.pibb.ac.cn

杨蓉，国家纳米科学中心研究员，博士生导师．2006 年于美国俄亥俄大学获得理学博士学位．2006～2007 年在美国明尼苏达大学化工材料系做博士后，2008 年起在国家纳米科学中心担任副研究员、研究员，从事材料、生物、化学和物理之间交叉的新兴科学的研究．研究工作涉及纳米功能材料的可控制备及组装，功能材料的表 / 界面结构、理化性质，及纳米功能材料的生物医学应用．在纳米材料的模拟酶特性及其应用研究领域也开展了一系列研究工作．作为项目负责人 / 项目骨干，主持 / 参与了多项国家级、中国科学院系统科研项目．在国际重要学术刊物上发表论文 50 余篇，获授权专利多项．

王琛，国家纳米科学中心研究员，博士生导师．1986 年毕业于中国科学技术大学，1992 年于美国弗吉尼亚大学获博士学位，1992～1993 年在美国亚利桑那州立大学从事博士后研究，1994 年被聘为华中师范大学教授，1995～2004 年在中国科学院化学所任研究员，2004 年至今为国家纳米科学中心研究员．长期从事扫描隧道显微术的原理及应用研究，纳米尺度上物质表面的物理和化学现象研究，在单分子物理化学及分子自组装等方面进行了系统和深入的研究．目前致力于研究基于多肽纳米结构的疾病检测与治疗技术．曾获得“国家杰出青年科学基金”资助、主持和参与了多项国家级科技项目．现任中国生物物理学会常务理事．在国际高水平学术刊物上发表论文 200 余篇，中英文论著 4 部．

Two-dimentional Transition-metal Dichalcogenide Nanocomposites as Novel Enzyme Mimics: An Overview*

YANG Rong[1,2)**], CAI Shuang-Fei[1)], WANG Chen[1,2)**]
([1)] *CAS Key Laboratory for Biomedical Effects of Nanomaterials and Nanosafety,CAS Center for Excellence in Nanoscience, National Center for Nanoscience and Technology, University of Chinese Academy of Sciences, Beijing* 100190, China;
[2)] *Sino-Danish College, University of Chinese Academy of Sciences, Beijing* 100190, China)

Abstract Nanozyme is a very exciting and promising field that aims to imitate the general principles of natural enzymes using various nanomaterials and offers a lot of practical applications in many areas. Natural enzyme has some intrinsic drawbacks such as high cost, low stability, difficulty in storage, and sensitivity of catalytic activity towards enviromental conditions. While, nanozyme demonstrates low cost, high stability and high efficient activity. Great progress has been achieved by various peroxidase and/or oxidase mimetics, This brief overview introduce the latest research progresses for two-dimentional transition-metal dichalcogenide nanocomposites as promising enzyme mimics.

Key words transition-metal dichalcogenide, nanocomposites, enzyme mimetics, peroxidases, biosensing
DOI: 10.16476/j.pibb.2017.0470

* This work was supported by grants from National Key R&D Program from the Ministry of Science and Technology of China (2016YFC0207102), The National Natural Science Foundation of China (21573050, 21501034) and Financial supports from Chinese Academy of Sciences (XDA09030303).
**Corresponding author.
YANG Rong. Tel: 86-10-82545616, E-mail: yangr@nanoctr.cn; WANG Chen. Tel: 86-10-82545561, E-mail: wangch@nanoctr.cn
Received: December 18, 2017 Accepted: January 20, 2018

Recently, nanozymes have evoked enormous research enthusiasm [1–3]. In comparison with natural enzymes, nanomaterial-based enzyme mimics have advantages of low costs, tunable catalytic activities, high stability against stringent reaction conditions, and ease of storage and treatment. Great progress has been achieved by various peroxidase and/or oxidase mimetics, such as the graphene oxide (GO)[4], carbon nanotubes[5], metal oxides[6–8], and monometallic Au[9–11] or bimetallic nanostructures[12–14], which could serve as promising candidates for natural enzyme in various applications.

Among the enzyme mimics, hybrid composite materials are particularly impressive and offer great opportunities for catalysis, since the combination of the respective properties of each component can achieve cooperatively enhanced performances. An increasing number of hybrid complexes with inorganic nanomaterials incorporated with different matrixes have been applied in catalysis [15–18]. Graphene-hemin composites[19–20], magnetic nanoparticle/CNT nanocomplexs [21], GO-Fe_3O_4 nanocomposites [22] and noble metal-graphene hybrids[23–24] have been proved to possess new and/or enhanced functionalities that cannot be realized by either component alone.

The successful investigation of graphene has attracted lots of attention to the graphene-like two-dimensional (2D) layered materials, such as layered transition-metal dichalcogenides (LTMDs) [25–30]. 2D TMDs are the MX_2-type compounds, where M is a transition-metal element and X a chalcogen, that is, S, Se, or Te [25]. One of typical materials is mono- and few-layer molybdenum disulfide (MoS_2), which has received significant attention because of its tunable energy bandgap and natural richness [31–32]. Recently, it has been reported that MoS_2 nanosheets possessed an intrinsic peroxidase-like catalytic activity, which could catalyze the oxidation of 3,3,5,5-tetramethylbenzidine (TMB) in the presence of hydrogen peroxide (H_2O_2) to produce a blue color [33–34]. The higher peroxidase-like activity with greater dispersity in aqueous solution of MoS_2-hemin nanosheet composites than hemin alone has also been demonstrated [35]. Moreover, a series of MoS_2-metal nanocomposites with enhanced peroxidase/oxidase-like activities and other multifunctionalities have been reported [36-38]. The biological applications of these materials are very promising.

Here, we give a brief overview on progress on 2D TMD nanocomposites with enhanced enzyme- like catalytic activities and their applications. The scope intends to cover the synthesis, mechanism of 2D TMD -based enzyme mimics, and their potential bio-chemical applications. Finally, both challenges and future perspectives of 2D TMD-based nanozymes are discussed for further study in the field.

1 The advantages of ultrathin 2D TMD nanocomposites

Ultrathin 2D nanocomposites show many unique physical and chemical properties [26]. Firstly, the confinement of electrons in two dimensions facilitates their remarkable electronic properties. Secondly, the large lateral size and atomic thickness endow their excellent flexibility, optical transparency, and ultrahigh specific surface area. This is very attractive for many surface-related applications such as electrocatalysis and biocatalysis. Thirdly, high exposure of surface atoms allows easy regulation to the properties and functionalities through element doping and surface modification.

Graphene is a single-atom-thick carbon film. One of the most useful properties of graphene is its excellent electronic properties. It has high charge carrier mobility at room temperature and excellent electrical conductivity, and is fundamentally and technologically interesting for a lot of applications [26]. However, the major drawbacks of graphene are the lack of a bandgap and its chemical inertness. It can only be made active by modifying with desired molecules, which results in the loss of some of its good properties. While, ultrathin 2D TMDs have versatile chemistry. Various kinds of 2D TMD nanosheets such as MoS_2, NbS_2, HfS_2, have different properties. For example, MoS_2 and WS_2 are semiconductors, NbS_2 is true metal, and HfS_2 is insulator. This offers new chances for fundamental and technological research in many fields including catalysis, energy storage and biosensing.

To potentially extend the functionalities of 2D TMD as versatile materials, modifying TMD with 0D metal nanoparticles (NPs) to form 2D-0D multifunctional hybrid materials is of great and widespread interest. Therefore, to design and fabricate 2D TMD nanocomposite-based new multifunctional hybrid nanomaterials with high enzyme-like activity would be helpful to expand their applications in biomedical fields, such as optical biosensors and

biocatalysts (Figure 1).

Among the 2D TMDs, MoS_2 is a molybdenite compound. Comparing to the indirect bandgap of 1.2 eV in bulk MoS_2, ulthathin MoS_2 has a direct bandgap of 1.8 eV [31−32]. This unique feature brings MoS_2 nanosheets significant improvement in optical and electronic properties. Besides the advantages of good chemical stability, high catalytic activity, low cost and environmental friendliness, the large surface areas of single-layer MoS_2 nanosheets make them excellent candidates for capturing numerous biomolecules and provides promising opportunities for the development of the signal amplification strategy, that should be extremely attractive in the area of biosensors.

Owing to abundant active edges and a large specific surface area, 2D TMD nanosheets also provides a promising support material for potential catalytic performance. Many monometallic NPs, such as Au, Ag, Pt and Co NPs have been successfully decorated on 2D TMD nanosheets. These TMD-NPs hybrid materials not only enhance the intrinsic properties of the materials but also bring novel properties and functions, thus providing great opportunities in developing novel optical sensors, advanced electrocatalysts, as well as biocatalysts[39−47].

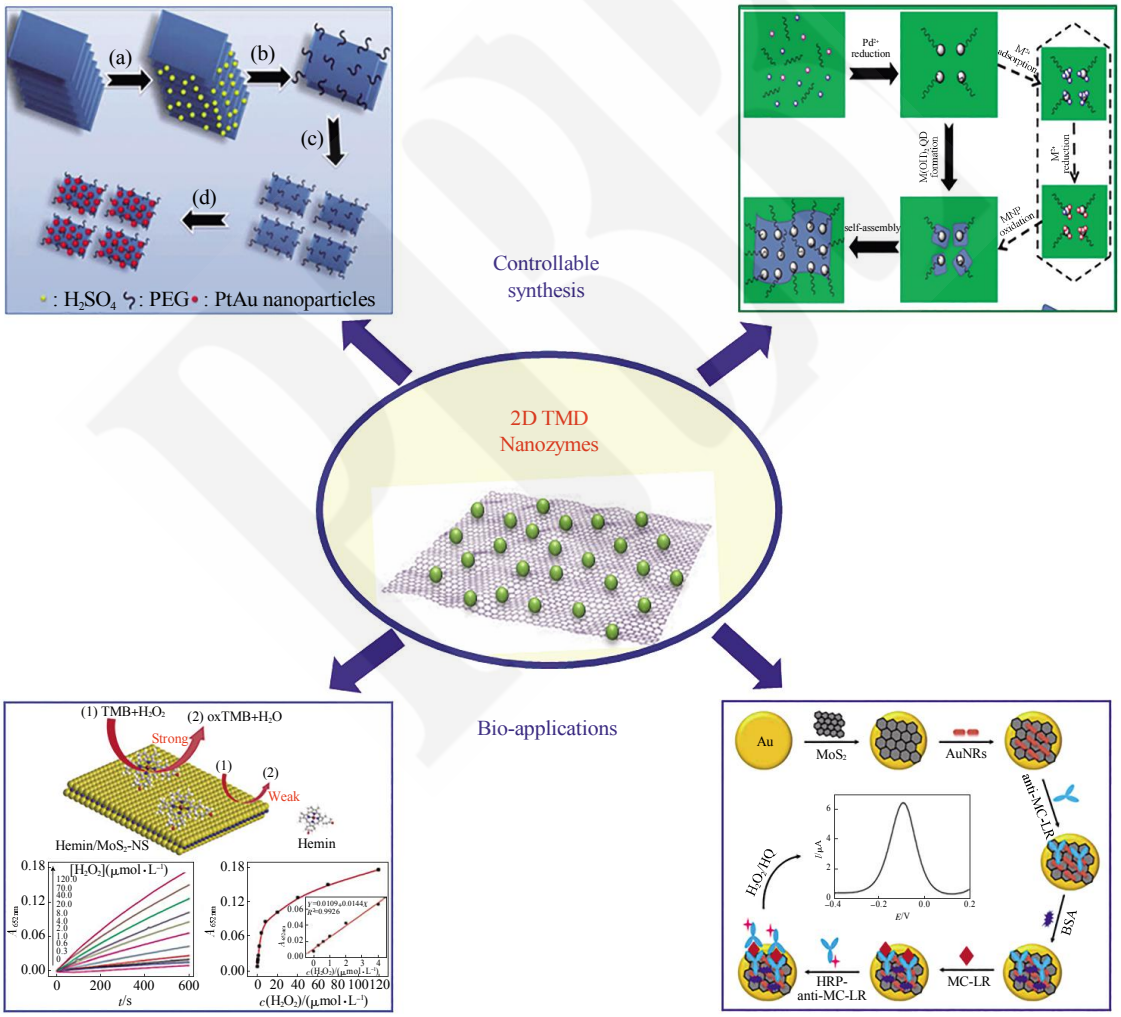

Fig. 1　2D TMD nanocomposites as novel enzyme mimics

2　Molybdenum disulfide (MoS_2), tungsten disulfide (WS_2) nanosheets as peroxidase mimetic catalysts

TMDs are layered materials of similar structure to graphite. TMDs can be exfoliated to single- or few-layer nanosheets. Among TMDs, MoS_2 is one of the most promising materials and exhibits unusual physical and electronic properties. Recently, Lin *et al.* [33] discovered that layered MoS_2 nanosheets

(Figure 2) possessed intrinsic peroxidase-like activity and could catalytically oxidize 3,3',5,5'-tetramethylbenzidine (TMB) by H_2O_2 to produce a color reaction. The catalytic activity followed the typical Michaelis-Menten kinetics and was dependent on temperature, pH, H_2O_2 concentration, and reaction time.

Based on the peroxidase-like properties of MoS_2 nanosheets, a highly sensitive and selective colorimetric method for H_2O_2 and glucose detection was developed (Figure 3). Moreover, a simple, inexpensive and portable test kit for the visual detection of glucose in normal and diabetic serum samples is developed by using agarose hydrogel as a visual detection platform. In their another work, Lin *et al*. found that the tungsten disulfide (WS_2) nanosheets also possessed intrinsic peroxidase-like activity[48]. And then, a colorimetric method and a portable testkit for the visual detection of blood glucose have been developed by using glucose oxidase (GOx) and WS_2 nanosheets catalyzed reactions.

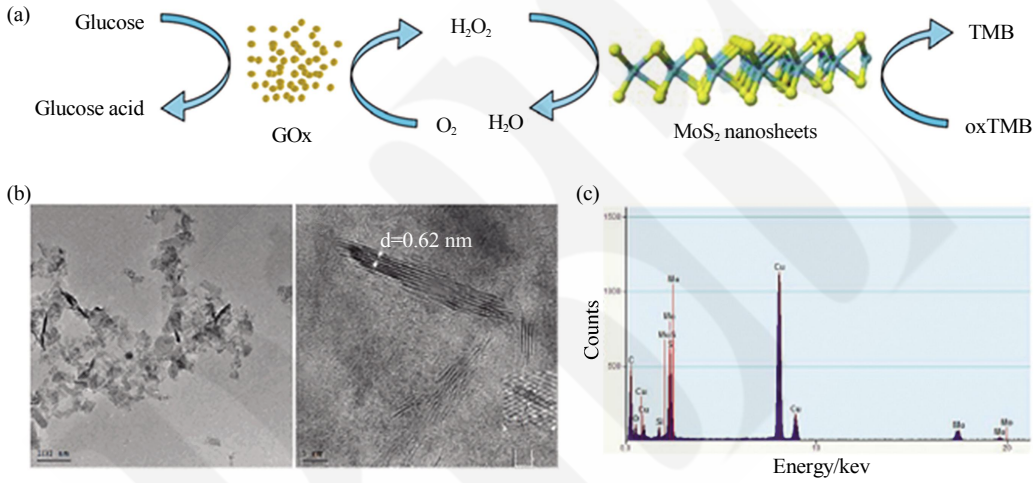

Fig. 2 Colorimetric detection of glucose by using glucose (GOx) and MoS_2 nanosheets

(a) Schematic illustration of colorimetric detection of glucose by using glucose oxidase (GOx) and MoS_2 nanosheet-catalyzed reactions. (b) TEM, HRTEM and EDX pattern of MoS_2 nanosheets[33].

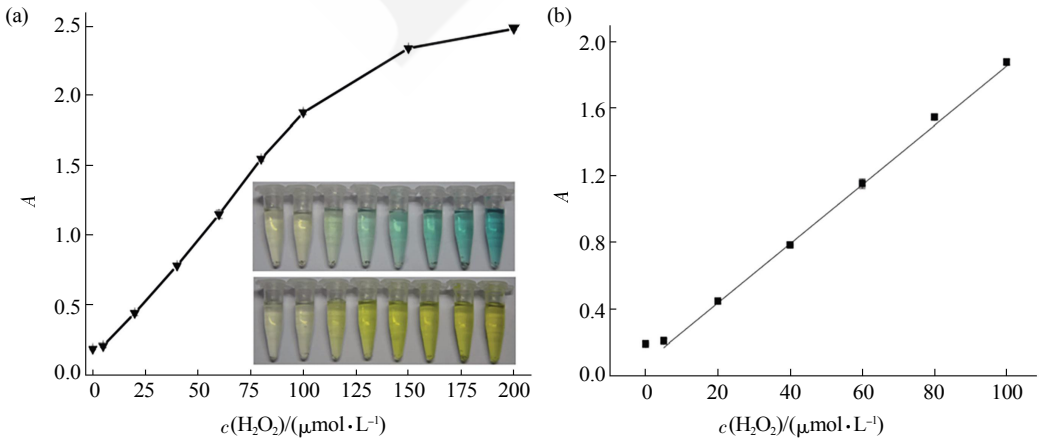

Fig. 3 H_2O_2 detection using MoS_2 nanosheets

(a) A dose-response curve for H_2O_2 detection and (b) the linear calibration plot for H_2O_2[33].

3 Non-metal functionalized MoS_2 nanosheets as peroxidase mimetic catalysts

3.1 MoS_2-PEG nanosheets

To improve the peroxidase-like activity of MoS_2 nanosheets, Zhao *et al* modified the MoS_2 nanosheet surface with polyethylene glycol (PEG) [49]. They prepared the MoS_2-PEG nanosheets with good water dispersiblity and stability using a liquid- phase exfoliation and pegylation process (Figure 4). Compared to the unmodified MoS_2 nanosheets, MoS_2-PEG nanosheets had better peroxidase-like catalytic activity, which was mainly manifested in the lower values of K_m and higher V_m. The apparent steady-state kinetic parameters also showed that the material increased the affinity between substrate and catalyst significantly.

Based on the good peroxidase-like property of MoS_2-PEG nanosheets, a colorimetric method for detection of H_2O_2 was developed with a limit of detection (*LOD*) of 1.18 μmol/L, which was comparable to that of the majority of the reported enzyme mimics of inorganic graphene analogues (Figure 5).

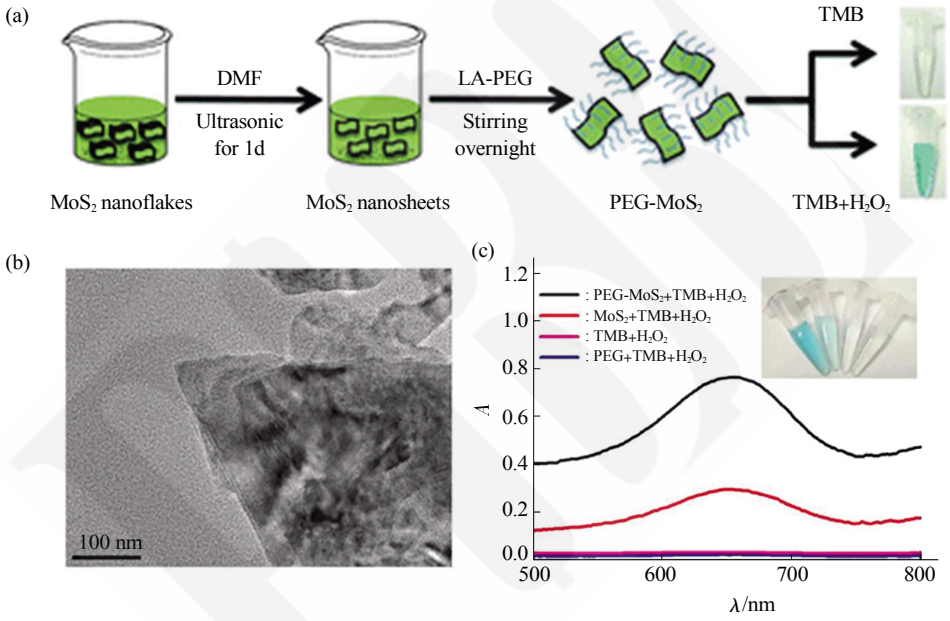

Fig. 4 Peroxidase-like activity of PEG-MoS_2 nanosheets

(a) Schematic illustration of synthetic process and peroxidase-like activity of PEG-MoS_2 nanosheets. (b) TEM image of PEG-MoS_2 nanosheets. (c) Peroxidase-like activity of different reaction systems. Inset: images of color changes (from left to right corresponding to MoS_2-PEG, MoS_2, blank control and PEG)[49].

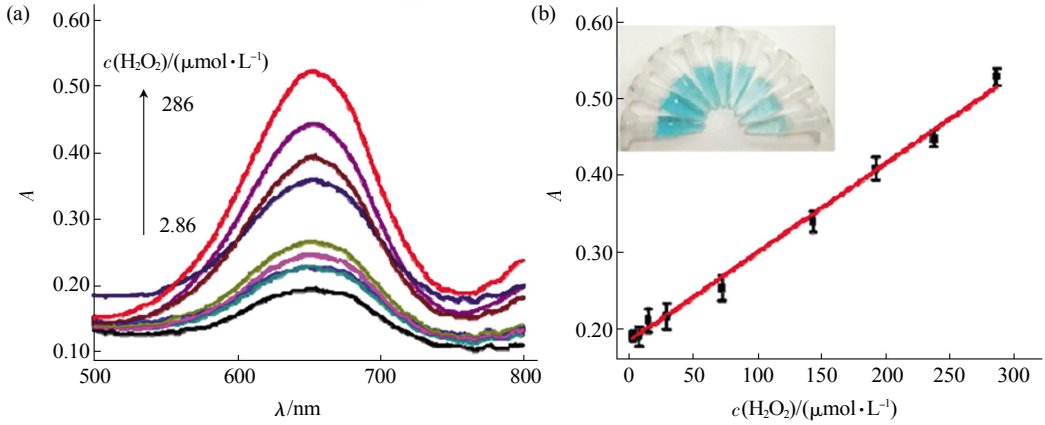

Fig. 5 H_2O_2 detection using PEG-MoS_2 nanosheets

(a) The UV-vis absorbance spectra changes in the presence of H_2O_2. (b) Linear calibration curve for H_2O_2 detection corresponding to (a). Inset: the photos of color change in this reaction system[49].

3.2 MoS_2-Hemin hybrid nanosheets

Hemin, an iron-protoporphyrin and the active center of the heme-protein family, is well-known for its properties of catalyzing a variety of oxidation reactions. Nevertheless, the direct use of hemin is challenging because of its molecular aggregation tendency in aqueous media and oxidative self-destruction in oxidizing media[50]. Taking this into account, Li *et al.*[51] prepared Hemin- functionalized MoS_2 nanosheets (MoS_2-hemin NSs) *via* van der Waals interactions between MoS_2 nanosheets (MoS_2-NSs) and hemin molecules in mixed methanol solution with sonication. The MoS_2-hemin NSs had high dispersity in aqueous solution, and exhibited a high catalytic activity in the oxidation of TMB in the presence of H_2O_2. It was found that when compared to MoS_2-NSs, the MoS_2-hemin NSs exhibited higher peroxidase-like activity (Figure 6).

On the basis of the intrinsic peroxidase property of MoS_2-hemin NSs, a novel H_2O_2 sensor was fabricated using spectrophotometry as shown in Figure 7a. Figure 7b showed the time-dependent absorption changes of TMB reaction solutions at 652 nm with different concentrations of H_2O_2 using MoS_2-hemin NSs as the catalyst. The absorbance of TMB reaction solutions increased with increasing H_2O_2 concentration. Figure 7c exhibited a typical H_2O_2 concentration-response curve under optimal conditions. The absorbance of reaction solution had a good linear relationship with the concentration of objective H_2O_2 in the range of 2.0×10^{-7} to 4.0×10^{-6} mol/L. The detection limit was calculated to be 4.3×10^{-8} mol/L.

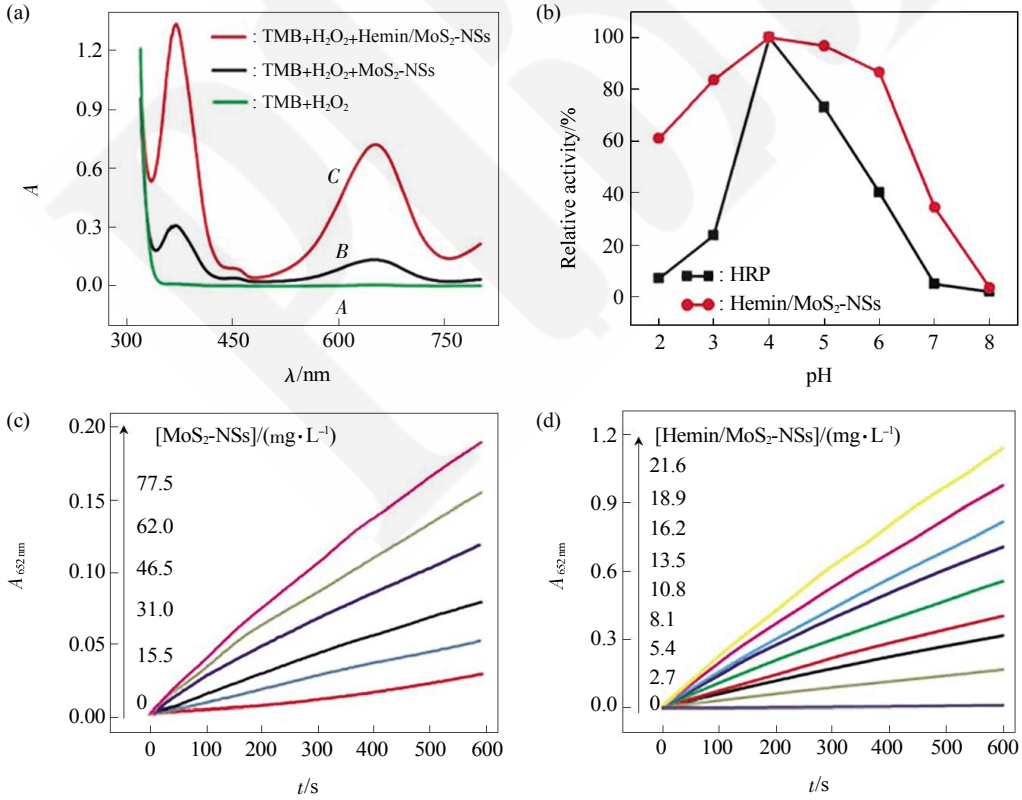

Fig. 6 Peroxidase-like activity of MoS_2-hemin NSs

(a) UV-vis absorption spectra of TMB reaction solutions (*A*) in the presence of MoS_2 NSs (*B*) or MoS_2-hemin NSs (*C*) after reaction for 10 min (pH 4.0). (b) Peroxidase-like activity of MoS_2- hemin NSs is dependent on pH. (c) Time-dependent absorption changes of TMB reaction solutions in the presence of different concentrations of MoS_2-NSs at room temperature and (d) Time- dependent absorption changes in the presence of different concentrations of MoS_2-hemin NSs at room temperature (pH 4.0)[51].

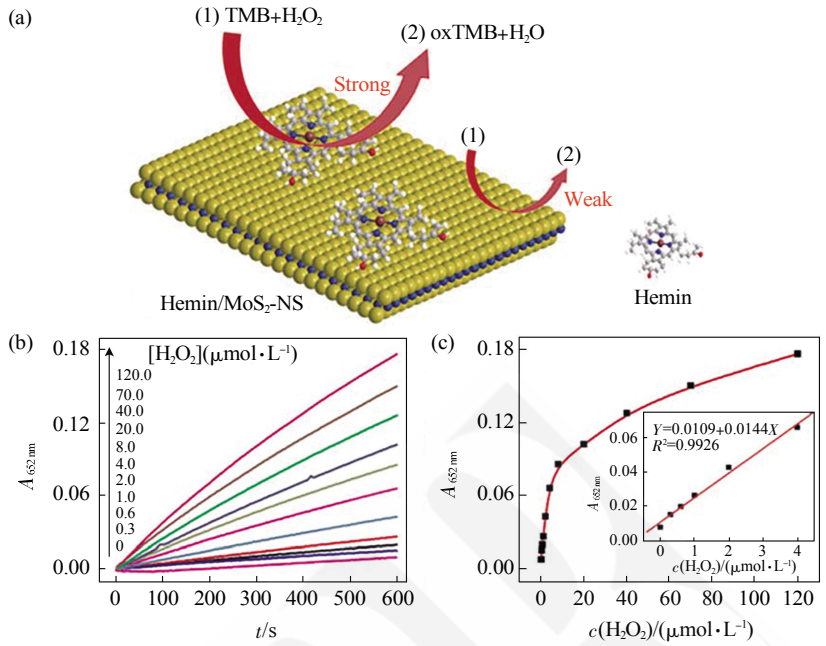

Fig. 7　The spectrophotometric detection of H_2O_2 using MoS_2-hemin NSs

(a) Schematic illustration of the spectrophotometric detection of H_2O_2 based on the catalytic activity of MoS_2-hemin NSs in TMB oxidation reaction. (b) Time-dependent absorption changes at 652 nm in the absence or presence of H_2O_2 in BR buffer (pH 4.0). (c) A dose-response curve for H_2O_2 detection using MoS_2-hemin NSs as an artificial enzyme. Inset: linear calibration plot for H_2O_2[51].

4　Metal nanoparticle-decorated MoS_2 nanosheets as peroxidase/oxidase mimetic catalysts

To improve the peroxidase-like activity of MoS_2, the surface modification such as combined with monometallic or bimetallic nanoparticles is of great and widespread interest. Bimetallic nanoparticles (BNPs) consist of two metals and often display enhanced catalytic performance than their monometallic counterparts because of synergistic effect[52–60]. Among them, Pt-based BNPs are presently being widely used as essential catalytic substances in various fields owing to the modified geometric and electronic structures of Pt. Cai *et al* decorated ultrathin MoS_2 nanosheets with a serious of BNPs to improve the efficiency of electron transfer to improve the peroxidase-like ability of MoS_2 nanosheets[36–38].

4.1　MoS_2-PtAg nanocomposites

4.1.1　Preparation and characterization of MoS_2-PtAg nanocomposites

A schematic illustration of the synthesis of MoS_2-PtAg nanocomposites is illustrated in Figure 8. In a typical experiment, the MoS_2 nanosheets were

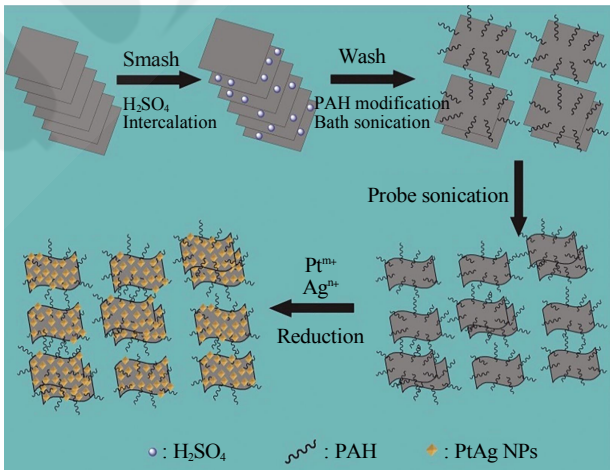

Fig. 8　Schematic illustration of synthesis of MoS_2-PtAg nanocomposites[36]

prepared through a liquid exfoliation method [36]. Briefly, commercial MoS_2 powder was intercalated with concentrated H_2SO_4. The intermediate was functionalized with a highly hydrophilic surfactant PAH through physical adsorption in water with sonication to obtain MoS_2-PAH nanosheets. Then, $H_2PtCl_6 \cdot 6H_2O$ and $AgNO_3$ as metal precursors were reduced by HCHO under hydrothermal conditions, and

PtAg alloy NPs were formed on the MoS_2-PAH nanosheets.

Figure 9 showed a typical TEM image of the MoS_2-PtAg nanocomposites with a Pt/Ag feeding molar ratio of 3∶1. The PtAg NPs were regularly octahedral with narrow size distribution and an average size about 13 nm, which were well dispersed on the MoS_2-PAH nanosheets. The HRTEM image in Figure 9b showed the lattice fringes with an inter-fringe distance of 0.23 nm, which was between the distance of face-centered cubic (fcc) Pt (0.226 nm) and Ag (0.236 nm) in the (111) plane. The result indicated the formation of PtAg alloy NPs on the MoS_2-PAH nanosheets. The crystalline structure of the MoS_2-PtAg nanocomposites was further examined by XRD (Figure 9c). The energy dispersive X-ray (EDX) analysis of MoS_2-PtAg showed that both the signals of Mo, S, Pt and Ag could be detected from these samples (Figure 9e). The analysed atomic ratio (Pt/Ag) by inductively coupled plasma optical emission spectroscopy (ICP-OES) was 74∶26, which was very close to the Pt/Ag feeding ratio of 3∶1. The element distributions of Mo, S, Pt and Ag in the nanocomposites were studied by a high-angle, annular dark-field scanning transmission electron microscope (HAADF-STEM). From the representative STEM image (Figure 9f) and its corresponding Mo, S, Pt and Ag elemental maps (Figure 9j), it could be seen that both Pt and Ag were evenly distributed in each individual NP. The chemical state of the as-prepared MoS_2-PtAg was confirmed by XPS (Figure 9j –m). Above results indicated that the ultrathin MoS_2-PAH nanosheets were successfully decorated with octahedral $Pt_{74}Ag_{26}$ alloy NPs.

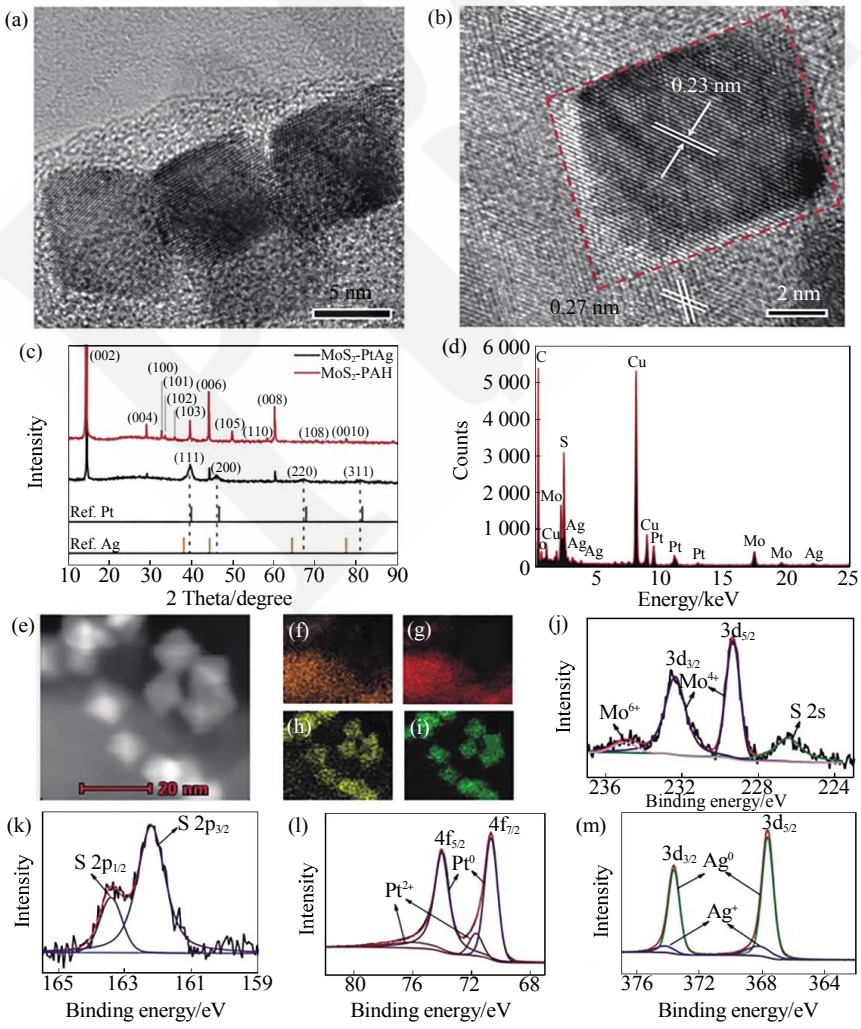

Fig. 9 Characterization of MoS_2-PtAg nanocomposites

Representative TEM image (a), HRTEM image (b), XRD pattern (c), EDX spectrum (d), High-angle annular dark-field scanning transmission electron microscope (HAADF-STEM) image (e), elemental maps for Mo (f), S (g), Pt (h) and Ag (i), peak-fitting XPS spectra of Mo 3d (j), S 2p (k), Pt 4f (l) and Ag 3d (m) regions of as-prepared MoS_2-PtAg nanocomposites[36].

4.1.2 Peroxidase-like activity and mechanism of MoS_2-PtAg nanocomposites

To investigate the catalytic activity of the MoS_2-PtAg nanocomposites, 3,3',5,5'- tetramethylbenzdine (TMB), 2,2-azino-bis (3-ethylbenzothiazoline-6-sulfonic acid) (ABTS) and *o*-phenylenediamine (OPD) were chosen as chromogenic substrates to study the peroxidase-like activities of MoS_2-$Pt_{74}Ag_{26}$. In the presence of H_2O_2, MoS_2-$Pt_{74}Ag_{26}$ nanocomposites could catalyze the oxidation of TMB, ABTS and OPD, producing the typical blue color for TMB, green color for ABTS and yellow color for OPD (Figure 10a), while the control experiments without MoS_2-$Pt_{74}Ag_{26}$ or without H_2O_2 showed negligible color variation (Figure 10b). This result indicated that MoS_2-$Pt_{74}Ag_{26}$ had peroxidase- like activity.

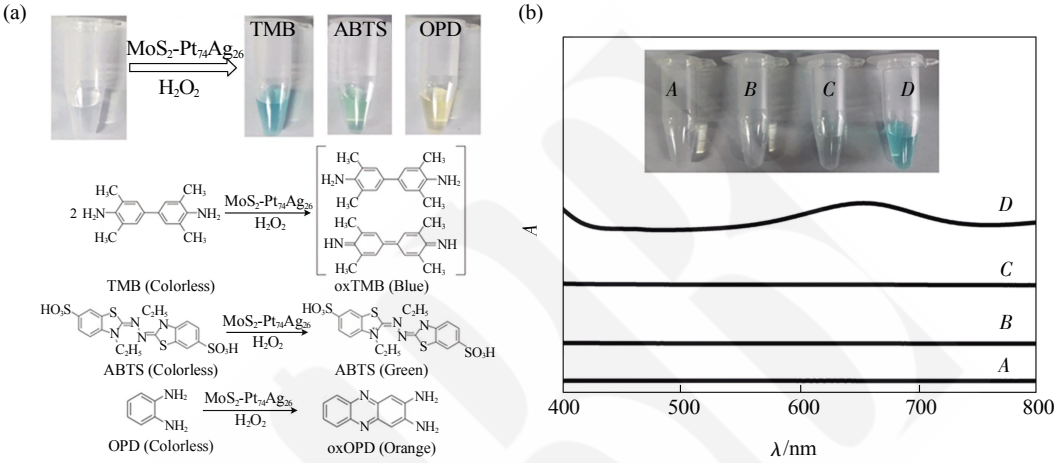

Fig. 10　The peroxidase-like activity of MoS_2-PtAg nanocomposites

(a) The color change and corresponding reaction schemes for the oxidation of TMB, ABTS and OPD catalyzed by the MoS_2-$Pt_{74}Ag_{26}$. (b) UV-Vis spectra of material solution (*A*), TMB solution (*B*), TMB-H_2O_2 solution (*C*) and TMB-H_2O_2-material solution (*D*) in 0.2 mol/L acetate buffer (pH 4.0). Inset: photographs of different solutions[36].

Similar to HRP, the catalytic activities of MoS_2-PtAg showed temperature, pH and H_2O_2 concentration dependence [36]. MoS_2-$Pt_{74}Ag_{26}$ displayed high catalytic activity at different over pH values (3.0–6.0) and a wide range of temperatures (20 ℃ –70 ℃), while the catalytic activity of HRP was largely inhibited after incubation at pH below 4.0 or at temperature higher than 50 ℃ [61]. Thus, the robustness of MoS_2-$Pt_{74}Ag_{26}$ made it potentially applicable under harsh conditions. For the catalytic oxidation of TMB by MoS_2-$Pt_{74}Ag_{26}$, the optimal pH was 4.0 and an optimal temperature was 50 ℃ . The peroxidase-like activity MoS_2-$Pt_{74}Ag_{26}$ was further investigated by the steady-state kinetic experiments. By monitoring the absorbance change at 652 nm for 30 min, typical Michaelis-Menten curves with TMB and H_2O_2 were obtained, respectively (Figure 11a,b). Michaelis-Menten constant (K_m) and maximum initial rate (v_{max}) were obtained using Lineweaver-Burk plot (Figure 11c,d).

Hydroxyl radical (•OH) as an important intermediate in peroxidase mimics-catalyzed colorimetric detections of H_2O_2 was studied extensively [1]. By adding terephthalic acid (TA) as fluorescent probe into the H_2O_2/MoS_2-$Pt_{74}Ag_{26}$ system, TA reacted with •OH for forming highly fluorescent 2-hydroxy terephthalic acid. As shown in Figure 12a, there was negligible fluorescence intensity without H_2O_2 or MoS_2-$Pt_{74}Ag_{26}$, while a emission peak at 425 nm appeared after MoS_2-$Pt_{74}Ag_{26}$ was added in the TA solution in the presence of H_2O_2, which indicated the production of •OH after the interaction between MoS_2-$Pt_{74}Ag_{26}$ and H_2O_2. The result showed that MoS_2-$Pt_{74}Ag_{26}$ could decompose H_2O_2 to generate the •OH radical. To further evaluate the effects of MoS_2-$Pt_{74}Ag_{26}$ on •OH signal intensity, a series of electron spin resonance (ESR) experiments in the 5,5-dimethyl-1-pyrroline *N*-oxide (DMPO) spin trap system had been carried out. As shown in Figure 12b, there were no apparent •OH signals in the

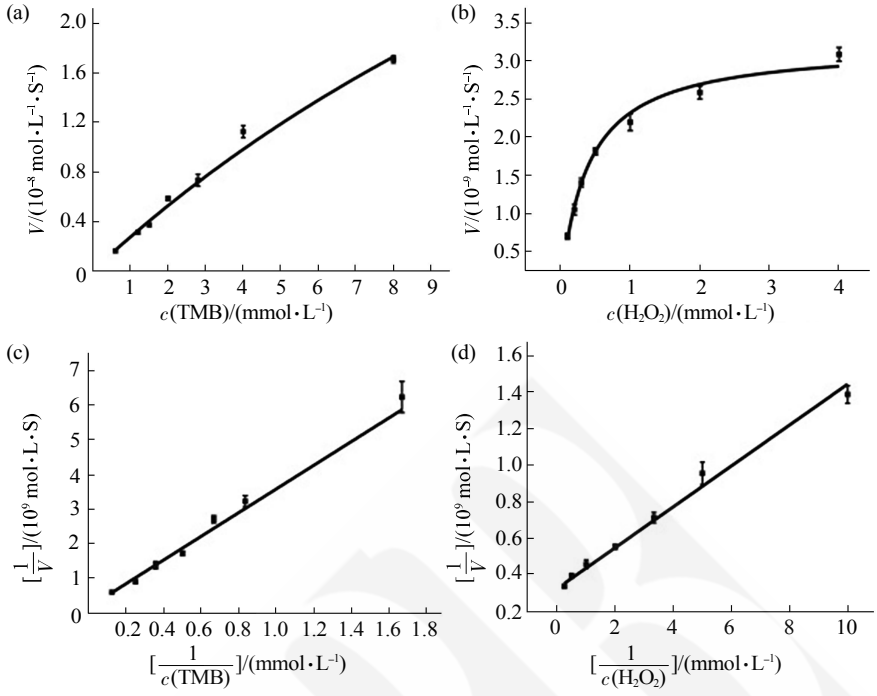

Fig. 11 Steady-state kinetic analysis

Steady-state kinetic analysis using Michaelis-Menten model (a, b) and Lineweaver-Burk model (c, d) for MoS_2-$Pt_{74}Ag_{26}$. The concentration of H_2O_2 was 1 mmol/L and TMB concentration was varied (a, c). The concentration of TMB was 1 mmol/L and H_2O_2 concentration was varied (b, d)[36].

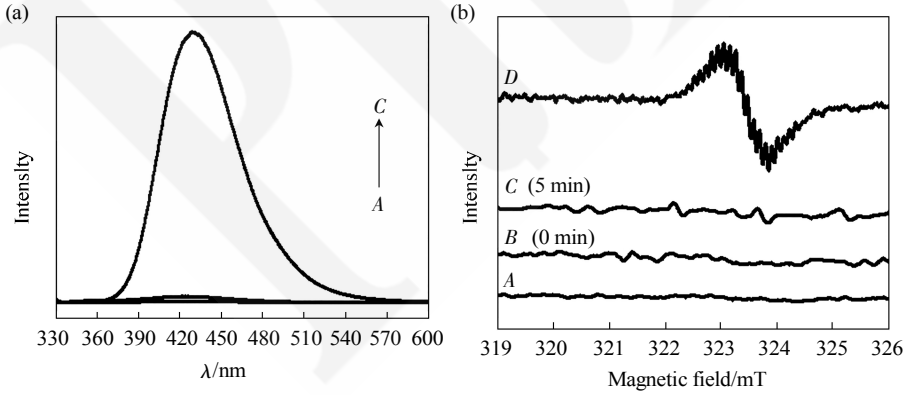

Fig. 12 The effect of MoS_2-PtAg on the formation of hydroxyl radical

(a) The effect of MoS_2-PtAg on the formation of hydroxyl radical with TA as a fluorescence probe. *A*: TA/MoS_2-$Pt_{74}Ag_{26}$; *B*: TA/H_2O_2; *C*: TA/MoS_2-$Pt_{74}Ag_{26}$/ H_2O_2. (b) ESR spectra for the oxidation of TMB catalyzed by MoS_2-PtAg: (*A*) Buffer/TMB/H_2O_2; (*B*–*C*) Buffer/H_2O_2/MoS_2-PtAg for 0 and 5 min; (*D*) Buffer/H_2O_2/MoS_2-PtAg/TMB[36].

buffer/TMB/H_2O_2 system. While, the intensity of •OH increased in the system of buffer/H_2O_2/MoS_2-$Pt_{74}Ag_{26}$ as time increased. However, after the addition of TMB to this solution, the signal of •OH disappeared. Instead, a strong TMB cation radical[62] signal could be detected. Above results indicated that MoS_2-$Pt_{74}Ag_{26}$ possessed peroxidase-like activity.

4.1.3 Applications: detection of H_2O_2 and glucose

Based on the intrinsic peroxidase property of MoS_2-$Pt_{74}Ag_{26}$, the detection of H_2O_2 and glucose was designed using the blue color reaction catalyzed by MoS_2-$Pt_{74}Ag_{26}$. Figure 13 showed the dependence of the absorbance at 652 nm on the concentration of H_2O_2, revealing that the intensity of absorption peak at

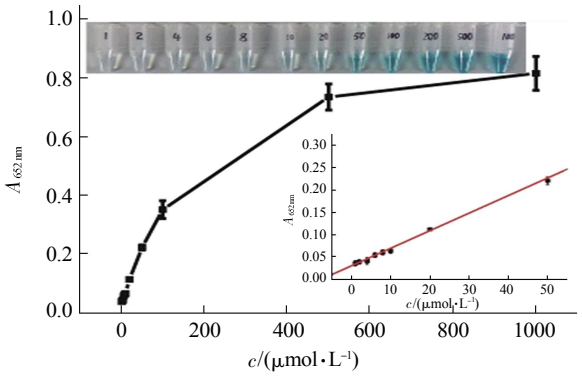

Fig. 13 Dependence of the absorbance at 652 nm on the concentration of H_2O_2 from 1 μmol/L to 1 mmol/L

The upper and lower insets show the corresponding photographs of different solutions and linear calibration plot, respectively[36].

652 nm increased with increased H_2O_2 concentration from 1 μmol/L to 1 mmol/L. The upper and lower insets of Figure 13 showed the corresponding photographs of different solutions and linear calibration plot, respectively.

The MoS_2-$Pt_{74}Ag_{26}$-based nanocomposite was also designed for detection of glucose. The dependence of the absorbance at 652 nm on the concentration of glucose from 1 μmol/L to 1 mmol/L was shown in Figure 14. The intensity of absorbance peak at 652 nm increased with increased glucose concentration. To examine the selectivity of present assay toward glucose, detection experiments had been performed in the presence of glucose analogue substances including glucose, fructose, lactose and mannitol. A blue color solution was obtained in the presence of glucose, however, no obvious blue color was observed for other compounds although their concentration is 5-fold higher than that of glucose (Figure 14b inset). Above observations indicated the designed sensing system exhibited excellent selectivity for glucose.

In summary, the MoS_2-$Pt_{74}Ag_{26}$ nanocomposites had been successfully prepared by a facile and efficient method and investigated as peroxidase mimics. A colorimetric method with high sensitivity and selectivity for H_2O_2 and glucose detection had been developed. The detections of H_2O_2 and glucose were in a linear range from 1×10^{-6} to 5×10^{-5} mol•L^{-1} and 1×10^{-6} to 1×10^{-5} mol•L^{-1}, respectively, with the detection limit down to 4×10^{-7} mol•L^{-1} for H_2O_2 and 8×10^{-7} mol•L^{-1} for glucose.

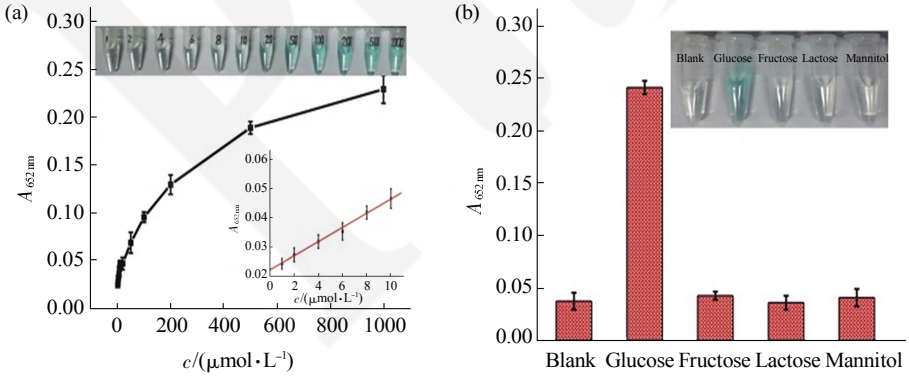

Fig. 14 Detection of glucose using MoS_2-PtAg nanocomposites

(a) Dependence of the absorbance at 652 nm on the concentration of glucose from 1 μmol/L to 1 mmol/L. The upper and lower inset show the corresponding photographs of different solutions and linear calibration plot, respectively. (b) Selectivity analysis of MoS_2-$Pt_{74}Ag_{26}$/GOx/TMB system for glucose detection by measuring the absorbance at 652 nm. Inset: photographs of different solutions. Inset: photographs of different solutions[36].

4.2 MoS_2-PtCu nanocomposites

4.2.1 Preparation and characterization of MoS_2-PtCu nanocomposites

Besides the MoS_2-PtAg nanocomposites, MoS_2-PtCu nanocompostes were also found had high peroxide catalytic properties [37]. The synthesis of MoS_2-PtCu nanocomposites was carried out without organic solvents or high temperature. The TEM image (Figure 15a) revealed that porous PtCu nanoparticles had a homogeneous distribution on the surface of MoS_2 nanosheets with an average size less than 20 nm. The crystal structure of MoS_2-PtCu was characterized by XRD (Figure 15c). HRTEM and XPS were further used to investigate the structure and element

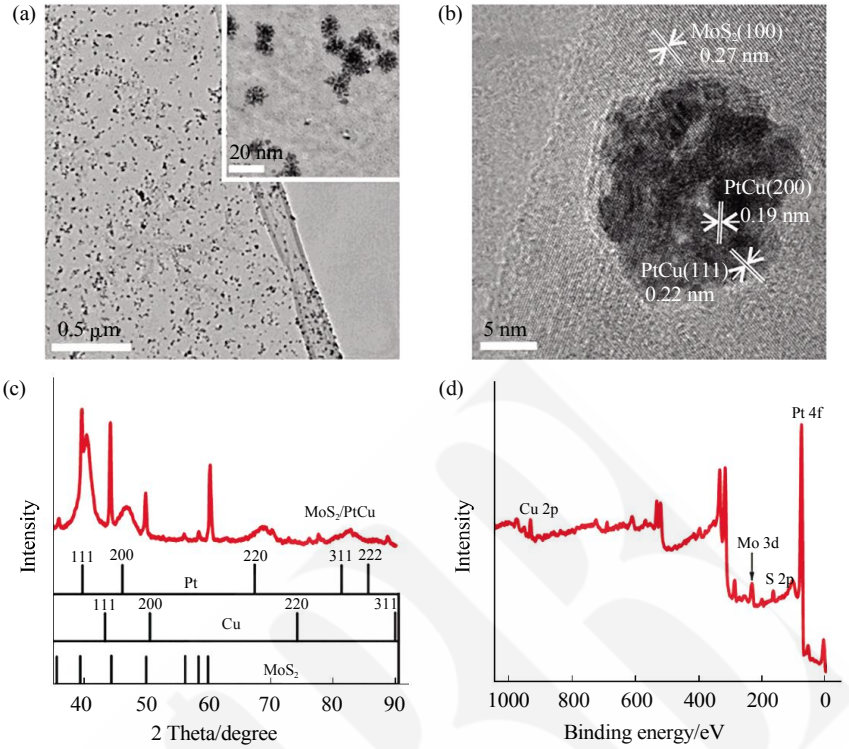

Fig. 15 Characterization of MoS_2-PtCu nanocomposites

(a) Representative TEM images, (b) HRTEM image, (c) XRD spectrum and (d) XPS spectrum of as-prepared MoS_2-PtCu nanocomposites[37].

distributions of the MoS_2-PtCu nanocomposites. As shown in HRTEM image (Figure 15b), the lattice spacing of 0.19 nm and 0.22 were corresponding to the (200) plane and the (111) plane of PtCu nanoalloys respectively. The lattice spacing of 0.27 nm was corresponding to the (100) plane of MoS_2 nanosheets. The nanocomposite content was also analyzed by ICP-OES. The element concentrations of Pt and Cu were 0.117 mmol/L and 0.016 mmol/L respectively. The atomic ratio of Pt∶Cu was 88∶12.

4.2.2 Enzyme-like activity of MoS_2-PtCu nanocomposites

The oxidase-like activity of MoS_2-PtCu nanocomposites was investigated in catalysis of the substrates ABTS, TMB and OPD. As shown in Figure 16, MoS_2-PtCu nanocomposites could quickly catalyze the oxidation of the three substrates without H_2O_2 in phosphate buffer, producing the typical colors. The control experiments without MoS_2-PtCu nanocomposites showed negligible color variation. Moreover, after bubbling MoS_2-PtCu nanocomposite dispersion with nitrogen to remove dissolved oxygen, the reaction rate of TMB oxidation decreased dramatically as shown in Figure 16. The above results indicated that MoS_2-PtCu nanocomposites exhibited an intrinsic oxidase-like activity, and the dissolved oxygen was the electron acceptors for the oxidation in the absence of H_2O_2.

Furthermore, the peroxidase-like activity of MoS_2-PtCu nanocomposites was also studied. After saturation with N_2 for 1.5 h to clear dissolved oxygen in buffer, MoS_2-PtCu nanocomposites could catalyze the oxidation of TMB in the presence of H_2O_2 to produce a blue color [37]. Like oxidase and other nanomaterials-based oxidase mimics, the catalytic activity of the nanoconjugates was also dependent on pH, temperature, and the concentration of substrates and catalyst. For the catalytic oxidation of TMB by using apt-MoS_2-PtCu, the optimal pH is 3.5. The nanoconjugates exhibited good stability and high oxidase-like activity over a broad temperature range (30℃–60℃).

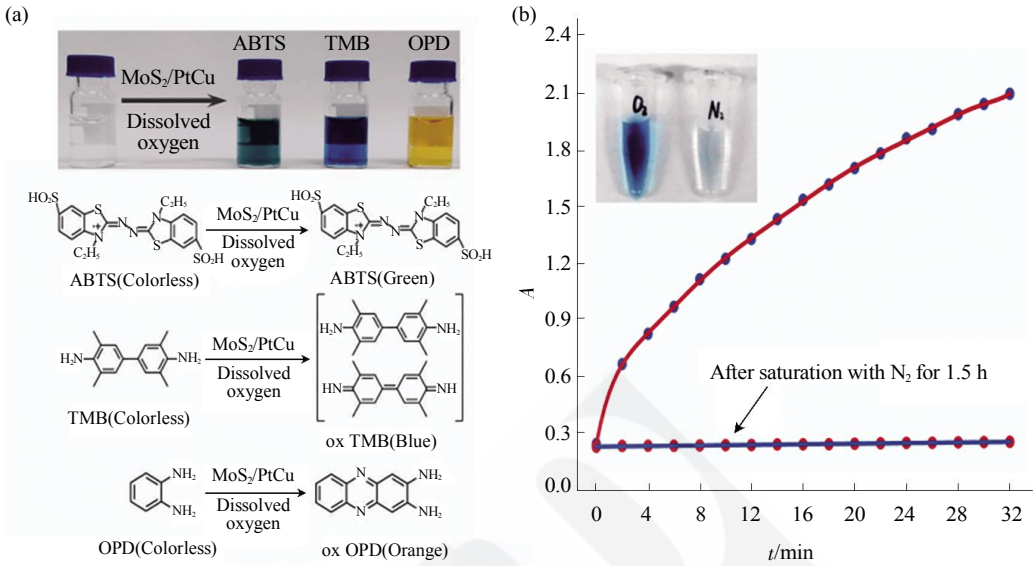

Fig. 16 The oxidase-like activity of MoS_2-PtCu

(a) Color evolution of ABTS, TMB and OPD oxidation by dissolved oxygen using MoS_2-PtCu as catalysts. (b) The oxidase-like activity of MoS_2-PtCu before and after saturation with N_2[37].

4.2.3 Applications: Aptamer-functionlizationed MoS_2-PtCu nanocomposites as cancer-cell immunoassay

A number of FA-functionalized colormetric biosensors had been reported to detect cancer cells [63–67]. However, most of the reported colorimetric biosensors needed to go through complicated covalent modifications. Simple and facile preparation processes for colorimetric biosensors are highly desired. Qi *et al*. [37] introduced streptavidin to MoS_2-PtCu nanocomposites *via* physical adsorption, then biotinylated aptamers were connected to surfaces. This approach appeared to be simpler, and provided a general surface modification method through biotin-streptavidin (STV) interactions. The nanocomposites were functionalized with a MUC1 aptamer termed S2.2 for cancer-cell detection [68–69]. MUC1 is a large transmembrane glycoprotein of the mucin family overexpressed on the surface of most epithelial cancers, such as breast, lung, prostate and ovarian cancer, *etc* [70–73]. The large surface-area-to-mass ratio of MoS_2 nanosheets and the negatively charged surface of MoS_2-PtCu nanocomposites provided a convenient way for absorption of STV without needs of other modifications. Biotinylated aptamer S2.2 was conjugated to MoS_2-PtCu *via* the adsorption of STV on the nanocomposites.

Figure 17 showed the working principle of the colorimetric biosensor based on aptamer-functionlizationed MoS_2-PtCu nanocomposites with high oxidase-like activity. On the basis of the oxidase-like activity of MoS_2-PtCu nanocomposites and MUC1 aptamers, elective binding apt-MoS_2-PtCu nanocomposites on the MUC1 overexpressed cells could convert the recognition process into quantitative colorimetric signal. This aptameric nanobiosensor had several advanced properties: (i) the preparation were

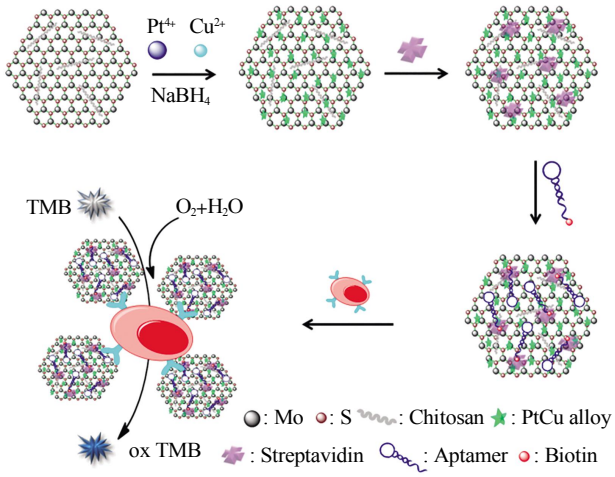

Fig. 17 Schematic representation of aptamer-functionlized MoS_2-PtCu colorimetric biosensor and its application for cancer-cell detection[37]

simple and rapid; (ii) the porous nanostructure could also increase the contact with substrates to enhance catalytic performance; (iii) the large surface area of single-layer MoS_2 nanosheets and large amounts of porous PtCu nanoparticles resulted in remarkable amplification of the colorimetric signal and improved sensitivity; (iv) this approach was simple and provided a general surface modification method through biotin-STV interactions. By altering different recognition elements, one could develop different colorimetric biosensors with desired demands.

By taking advantage of the oxides-like activity, selective binding apt-MoS_2-PtCu on the tumor cells can convert the recognition process into quantitative colorimetric signal. For the colorimetric detection of cancer cells, it was first studied whether S2.2 aptamer functionalized MoS_2-PtCu (apt-MoS_2-PtCu) could efficiently differentiate between target cells and control cells. In this study, two MUC1-negative cells (HEK293 and HepG2) [74–76] and two MUC1 overexpressed cells (MCF-7 and A549) [77–78] were between target cells and control cells, which suggested that apt-MoS_2-PtCu could bind selectively to MUC1 overexpressed cells employed as control groups and target cells respectively. As shown in Figure 18a, an obvious difference of absorbance was observed (MCF7 and A549) and catalyze a color change reaction in the presence of TMB. The above results also indicated that the nanoconjugates could give specific response to cancer cells with different level of MUC1-protein expression.

To further demonstrate the selectivity to target cells through the interaction between MUC1 proteins and S2.2 aptamers, random DNA modified MoS_2-PtCu nanoconjugates (ram-MoS_2-PtCu) was prepared and free S2.2 aptamers were used to locate the binding sites. As a result (Figure 18b), the absorbance of apt-MoS_2-PtCu with MCF7 cells was significantly higher than the same amount of MoS_2-PtCu or ram-MoS_2-PtCu with MCF7cells. The nanoconjugates were then used for quantitative colorimetric detection of MUC1 overexpressed cells (MCF7). In the presence of TMB, the apt-MoS_2-PtCu conjugated cells catalyzed a color reaction that could be judged by the naked eye easily and be quantitatively monitored by the absorbance change at 652 nm (Figure 18c). As the number of target cells increased, the absorbance at 652 nm changed rapidly, suggested that the increasing number of target cells translates into an increasing number of MUC1 proteins available for binding to apt-MoS_2-PtCu nanocomposites. Using this method, as low as 300 MCF7 cells could be detected, demonstrating good sensitivity of the method.

In summary, the MoS_2-PtCu nanocomposites with excellent oxidase-like activity had been prepared. By taking advantage of MUC1 aptamer conjugated MoS_2-PtCu, a sensitive and selective colorimetric aptasensor for cancer-cell detection based on the oxides-like activity of MoS_2-PtCu nanocomposites was developed. As the preparation processes of the proposed aptasensor were easy and time-saving, this work would facilitate the utilization of MoS_2-PtCu with intrinstic oxidase activity in bioassays and biotechnology by altering different recognition elements with the practical demands, such as aptamers, nuclei acids, antibodies and peptides.

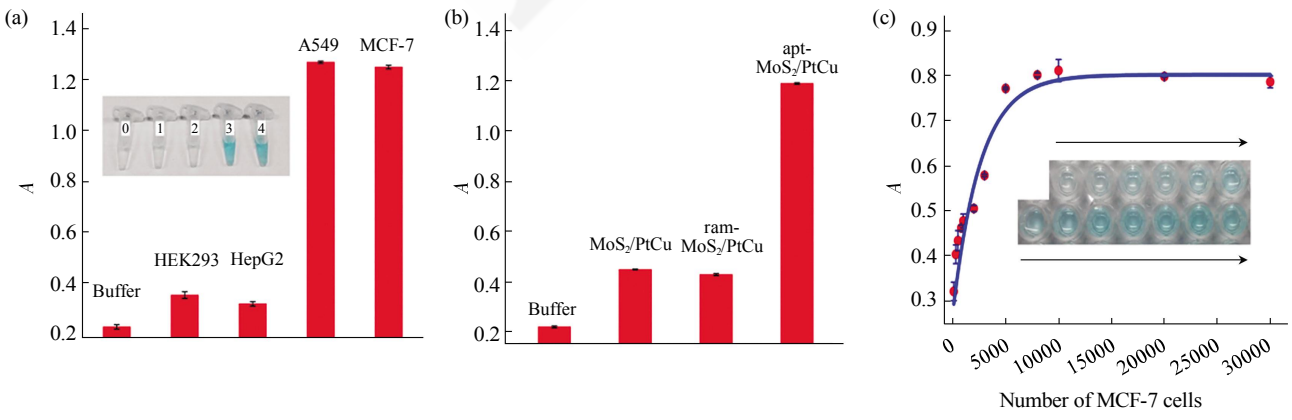

Fig. 18 Detection of MCF-7 cells using apt-MoS_2-PtCu

(a) Response of different cells using apt-MoS_2-PtCu to TMB. (b) Colorimetric response of MCF7 after incubation with different nanocomposites (ⅰ : no nanocomposites; ⅱ : MoS_2-PtCu; ⅲ : ram-MoS_2-PtCu; ⅳ : apt-MoS_2-PtCu). (c) The absorption values at 652 nm after incubation with apt-MoS_2-PtCu depend on the number of MCF-7 cells[37].

4.3 MoS_2-PtAu nanocomposites

4.3.1 Preparation and characterization of MoS_2-PtAu nanocomposites

The strategy to prepare MoS_2-PtAu nanocomposites was illustrated in Figure 19. MoS_2 NSs were firstly prepared *via* a modified liquid exfoliation method by using H_2SO_4 intercalation and sonication [38]. Subsequently, the MoS_2 NSs were functionalized with PEG through physical adsorption. Finally, metal precursors were reduced by one-pot strategy in the MoS_2-PEG NS dispersion.

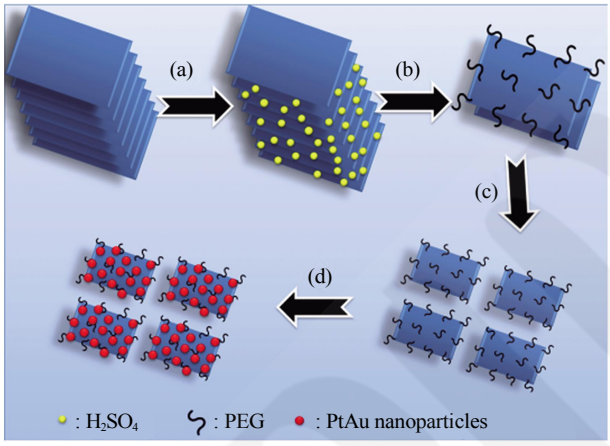

Fig. 19 Schematic illustration of synthesis of MoS_2-PtAu nanocomposite

(a) H_2SO_4 intercalation; (b) Exfoliation and surface modification of MoS_2 with PEG; (c) Probe sonication of MoS_2 nanosheets and (d) Reduction of metal precursors by $NaBH_4$[38].

Typical TEM images of the MoS_2-Pt_3Au nanocomposites were shown in Figure 20a , and one can see that spherical PtAu NPs are well-dispersed on MoS_2-PEG NSs. The nanocomposites could be well-dispersed in water (Figure 20a inset). The HRTEM image in Figure 20b showed the lattice fringes with an inter-fringe distance of 0.23 nm, which was between the distance of face-centered cubic (fcc) Pt (0.226 nm) and Au (0.235 nm) in the (111) plane. Also, the lattice spacing of 0.27 nm belongs to the (100) plane of MoS_2[79] could be observed in the same image. The XRD diffraction peaks of PtAu in the sample (Figure 20c) located between those of the standard peaks of Pt and Au, demonstrating the formation of PtAu alloys. The element distributions of Mo, S, Pt and Au in the nanocomposites were studied by a HAADF-STEM. From the representative STEM image (Figure 20d) and its corresponding elemental maps (Figure 20e –h), it could be seen that these elements were evenly distributed in the nanocomposites. This observation was supported by EDX, in which the signals of Mo, S, Pt and Au elements could be detected (Figure 20i).

The high-resolution Mo 3d XPS spectrum could be deconvoluted into three single peaks (Figure 21a). The two peaks at 232.5 eV ($3d_{3/2}$) and 229.4 eV ($3d_{5/2}$) binding energies are attributed to Mo^{4+}, while the shoulder at 226.5 eV can be assigned to S 2s.

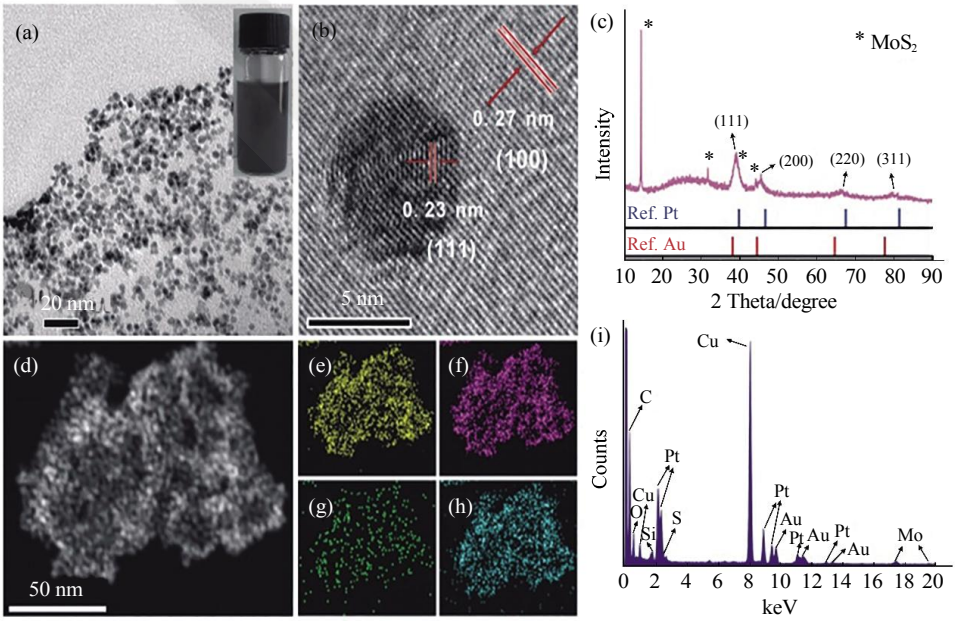

Fig. 20 Characterization of MoS_2-Pt_3 Au nanocomposites

(a) Typical TEM image (Inset shows a photograph of the nanocomposites dispersed in water), (b) HRTEM image, (c) XRD pattern, (d) HAADF-STEM image, elemental maps for (e) Au, (f) Pt, (g) Mo and (h) S, (i) EDX spectrum of MoS_2-Pt_3Au_1 nanocomposites[38].

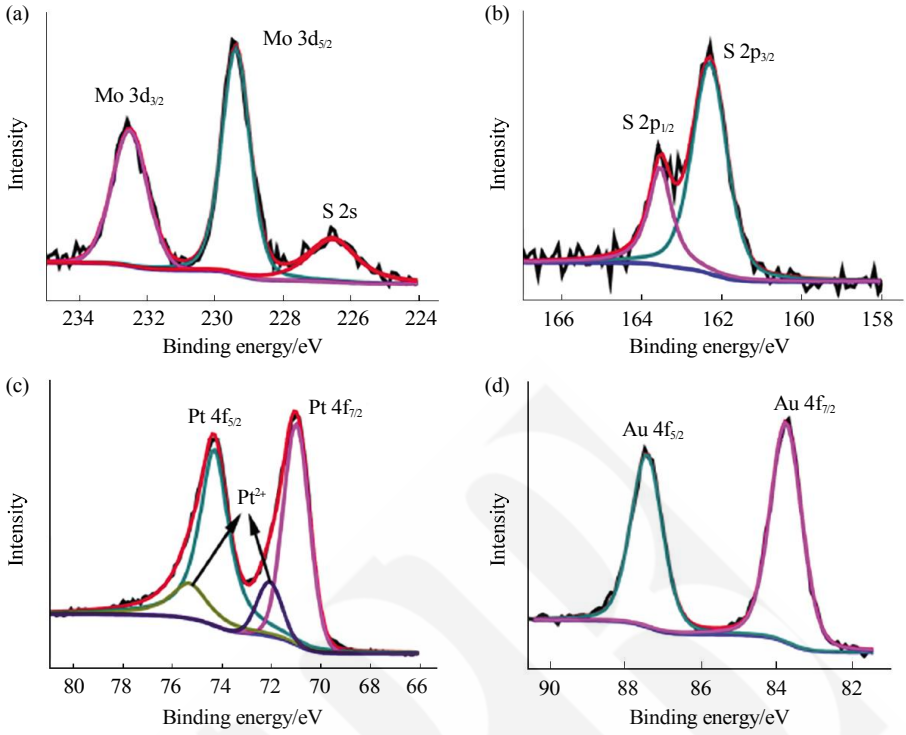

Fig. 21 High-resolution peak-fitting XPS spectra of Mo 3d(a), S 2p(b), Pt 4f(c) and Au 4f(d) regions of the MoS_2-Pt_3Au nanocomposites[38]

Additionally, the S 2p spectrum shows two peaks located at 163.5 eV and 162.3 eV (Figure 21b), which are characteristics of the S $2p_{1/2}$ and S $2p_{3/2}$ components of MoS2, respectively[37]. Meanwhile, XPS spectrum of Pt 4f (Figure 21c) displays two peaks at 74.3 eV ($4f_{5/2}$) and 71.0 eV ($4f_{7/2}$), which is indicative of elemental Pt^0. The Au 4f spectrum (Figure 21d) consists of two individual peaks at 87.4 eV ($4f_{5/2}$) and 83.8 eV ($4f_{7/2}$), which can be assigned to the Au^0 [80]. Taken together, the few-layer MoS_2-PEG NSs were successfully decorated with PtAu NPs.

4.3.2 Catalytic activities and mechanism of MoS_2-PtAu nanocomposites

The catalytic properties MoS_2-PtAu nanocomposites were investigated with TMB oxidation (Figure 22). In the absence or presence of H_2O_2, it was found that MoS_2-Pt_3Au_1 could catalyze the oxidation of TMB, producing a typical blue color with the maximum absorbance at 652 nm, while the control experiments without nanocomposites showed negligible color variation. These results indicate that the nanocomposites had oxidase- and peroxidase-like activities. Compared to pure supports, an approximate 3-fold enhancement in oxidase- or peroxidase-like activity of nanocomposites was observed. The excellent enzyme mimic activities of our nanocomposites can be attributed to both abundant active sites of Pt_3Au_1 NPs and a large surface area of MoS_2-PEG NSs, which are beneficial to the adsorption of TMB molecules and subsequent electron transfer from TMB to nanocomposites, resulting in the oxidation of TMB molecules. Among the various MoS_2-Pt_xAu_y nanocomposites, MoS_2-Pt_3Au possessed the highest activity. Thus, it was chosen as a typical enzyme mimic for further studies.

To optimize the reaction conditions, several important parameters including medium pH, incubation temperature, nanocomposite concentration and H_2O_2 concentration were investigated. MoS_2-Pt_3Au nanocomposites displayed high activities over a wide range of pH (3.0–7.0) and mild temperature (20℃–60℃). The optimal pH and temperature of the MoS_2-Pt_3Au nanocomposites were 4.0 and 35℃, respectively [38]. To get an insight into the reaction mechanism, a series of control experiments for TMB oxidation without H_2O_2 were first carried out. As shown in Figure 23a, it was found that the reaction rate increased with an increase in nanocomposite

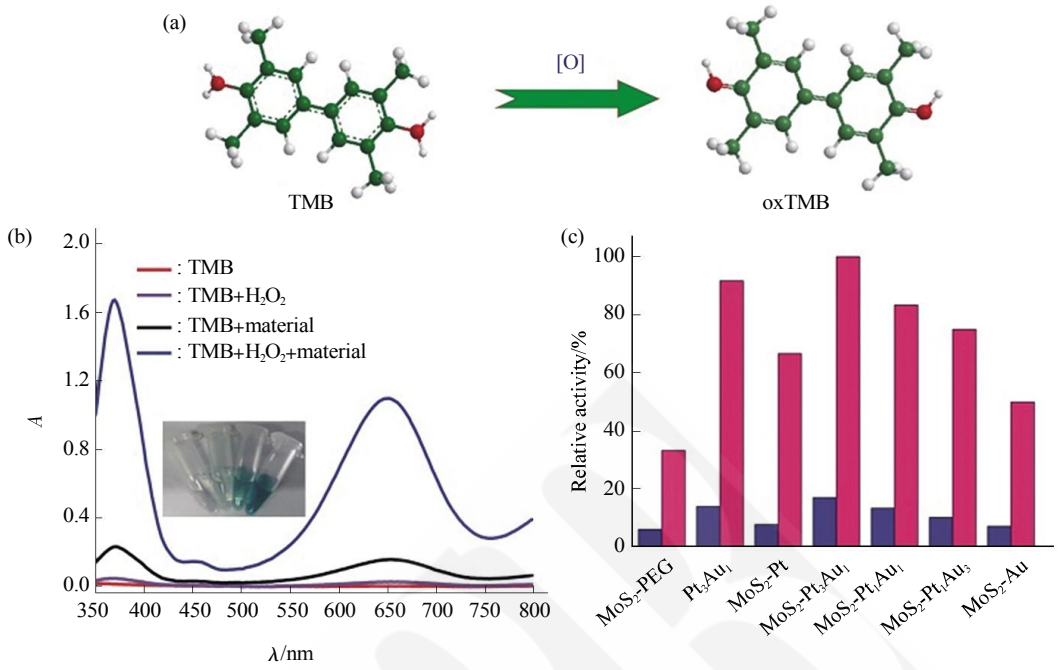

Fig. 22　Catalytic activities of MoS_2-PtAu nanocomposites

(a) Scheme of TMB oxidation, (b) TMB oxidation catalyzed by MoS_2-Pt_3Au nanocomposites (inset shows corresponding photographs of different solutions) and (c) comparison of catalytic activities of different materials. Blue and pink bars represent the oxidase- and peroxidase-like activities, respectively[38].

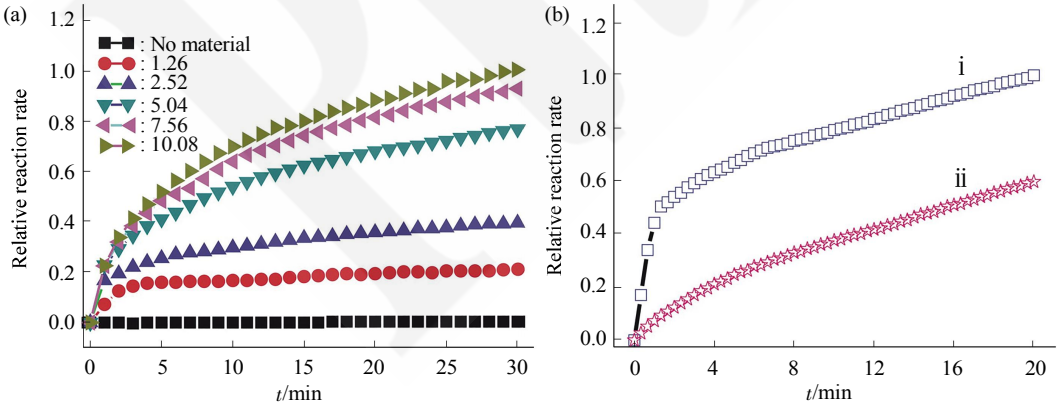

Fig. 23　TMB oxidation experiments

(a) Effect of hybrid concentration (mg·L^{-1}) on TMB oxidation; (b) Effect of dissolved oxygen or saturation with N_2 on TMB oxidation: (i) in air; (ii) after saturation of hybrids with N_2, reaction was carried out in air[38].

concentration. Moreover, reaction performed after saturation with N_2 gave rise to a quick decrease in the rate (Figure 23b). The result suggested that oxygen should be involved in the oxidation reaction, where the dissolved oxygen acted as electron acceptors. It is believed that the mechanism was similar to that of oxygen reduction reaction (ORR) in electrochemistry, in which electrons transferred from TMB molecules to nanocomposites, leading to reduction of the adsorbed oxygen and simultaneous oxidation of TMB. For TMB-H_2O_2-material system, a similar process occurred which H_2O_2 were electron acceptors.

4.3.3　Applications: colorimetric detection of phenol

With excellent activity and high stability

indicated above, MoS_2-Pt_3Au holds great promise in detection of small molecules. Accordingly, to explore the potential of MoS_2-Pt_3Au as a peroxidase mimic in the detection of organic molecules, a colorimetric detection of phenol was designed. The assay was based on oxidative coupling of phenol and 4-AAP to generate a pink quinoid type dye, which exhibited a characteristic absorption peak at 505 nm. The coupling reaction was carried out in acetate buffer under ambient conditions. In the absence of nanocomposites and H_2O_2, the solution showed almost no color transformation (Figure 24), while nanocomposites alone gave a weak pink color. After addition of nanocomposites and H_2O_2, the reaction solution changed from colorless to deep red with a dramatic increase in the absorbance at 505 nm. Thus, the combination of MoS_2-Pt_3Au nanocomposites and H_2O_2 was employed in the further studies.

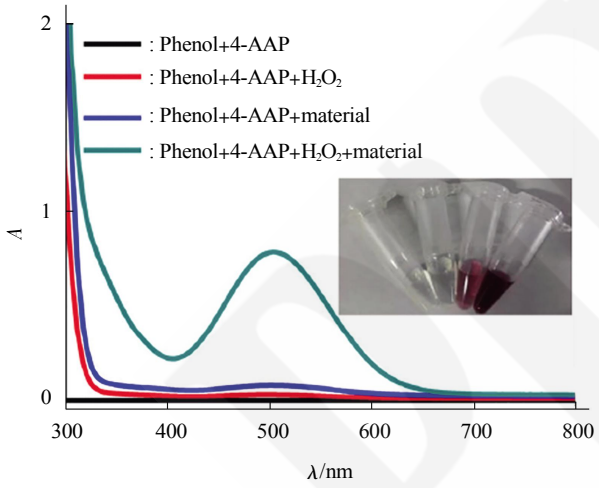

Fig. 24 UV-Vis spectra of solutions of oxidative coupling of phenol and 4-AAP catalyzed by MoS_2-Pt_3Au_1

Inset shows corresponding photos of different solutions (from left to right)[38].

Under the optimal conditions, the method developed was used for phenol detection. Figure 25a shows a typical phenol concentration response curve where as low as 0.2 μmol/L phenol (signal-to-noise ratio =3) could be detected with a linear range from 4 μmol/L to 1 mmol/L. The result indicates that this method could be used to detect the content of phenol.

To evaluate selectivity of this analytical strategy, a series of control experiments were carried out using various commonly-used organic molecules including alcohols, amines, and so on. The concentration of these control molecules was 50 times high than that of phenol. However, no obvious color variation could be observed in the control samples (Figure 25b). Thus, the present colorimetric method has a high selectivity towards phenol detection. Encouraged by high sensitivity and selectivity of our assay, the colorimetric method based on MoS_2-Pt_3Au is likely to be capable of practically useful phenol detection.

In summary, MoS_2-PtAu nanocomposites composed of PtAu NPs decorated few-layer MoS_2 NSs were controllably fabricated. The MoS_2-Pt_3Au nanocomposites displayed enhanced enzyme mimic activities, resulting from the synergistic effect of MoS_2-PEG nanosheets and Pt_3Au nanoparaticles. With these findings, a simple, fast and low-cost colorimetric detection of phenol with high selectivity was developed based on the competitive oxidation of TMB and these interfering substances.

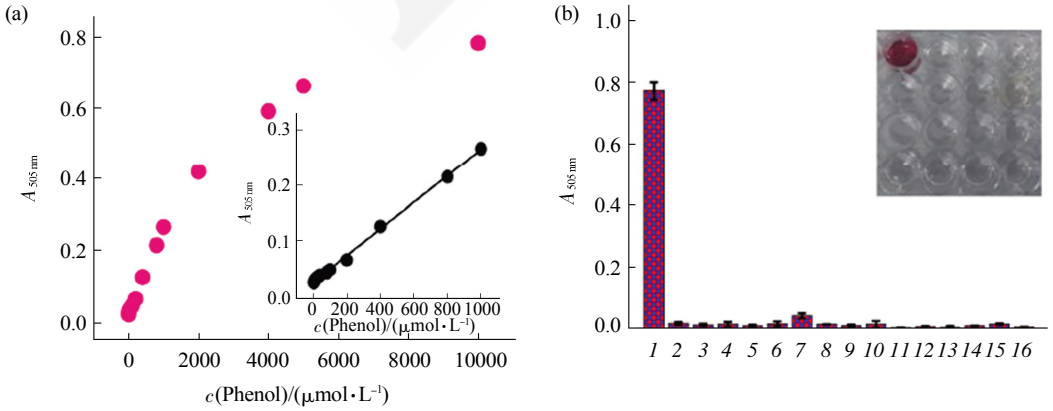

Fig. 25 Selectivity of phenol detection

(a) Linear calibration of the reaction system at varied phenol concentrations. (b) Determination of selectivity of phenol detection (from left to right): (*1*) Phenol; (*2*) Methanol; (*3*) Ethanol; (*4*) 2-propanol; (*5*) Ethylene glycol; (*6*) Diethylene glycol; (*7*) Benzylalcohol; (*8*) Aniline; (*9*) Octylamine; (*10*) Toluene; (*11*) 1-methylimidazole; (*12*) N,N-dimethylformamide; (*13*) Tetrahydrofuran; (*14*) Dimethyl sulphoxide; (*15*) Ethyl acetate and (*16*) N-methyl pyrrolidone[38].

5 Other layered MoS_2-based nanomposites as peroxidase mimetic catalysts

Sun *et al.* [81] synthesized Au-Pd NPs with core-shell structure on exfoliated MoS_2 nanosheets, and showed that the prepared Au-Pd/MoS_2 hybrid exhibits peroxidase-like properties towards the oxidation of TMB. They also found that the nanocomposites with Au-Pd mass ratio of 1∶2 (MoS_2-Au_1Pd_2) exhibited the highest catalytic activity due to the synergic effect between the Au-Pd nanoparticles and MoS_2 support as shown in Figure 26.

Nirala *et al.* [82] took advantage of the peroxidase-like activity of both MoS_2 nanoribbons and gold nanoparticles for synergistically enhanced colorimetric detection of cholesterol. The proposed MoS_2 NRs-AuNPs system could realize quick and reliable detection of free cholesterol using unaided eye with a line arrange from 0.04 to 1 mmol/L and a detection limit of 0.015 mmol/L (Figure 27).

Besides, Peng *et al.* [83] demonstrated that MoS_2/GO possessed intrinsic and light-enhanced peroxidase-like activity. The high catalytic activity of MoS_2/GO could be attributed to its high conductivity

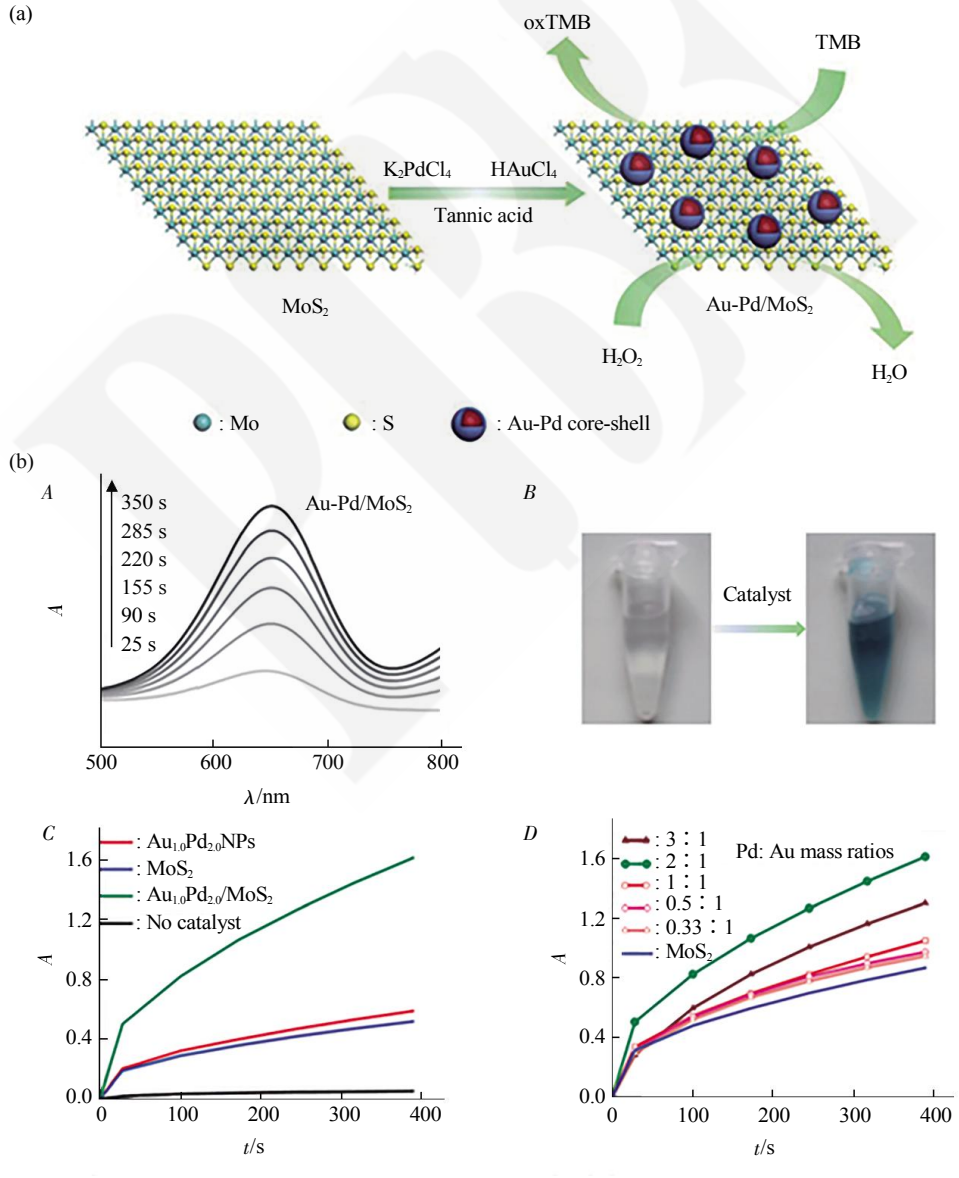

Fig. 26　TMB catalytic oxidation by Au-Pd/MoS_2 hybrids

(a) Illustration for the preparation of Au-Pd/MoS_2 hybrids and its catalytic oxidation of TMB. (b) The evolutions of absorbance spectra (*A*) and colour evolution (*B*) of TMB oxidation over time in the presence of Au-Pd/MoS_2 hybrid, (*C*) time- dependent absorbance changes at 652 nm using NPs and substrate, (*D*) time-dependent absorbance changes at 652 nm using Au-Pd/ MoS_2 hybrids with different Au-Pd mass ratios[81].

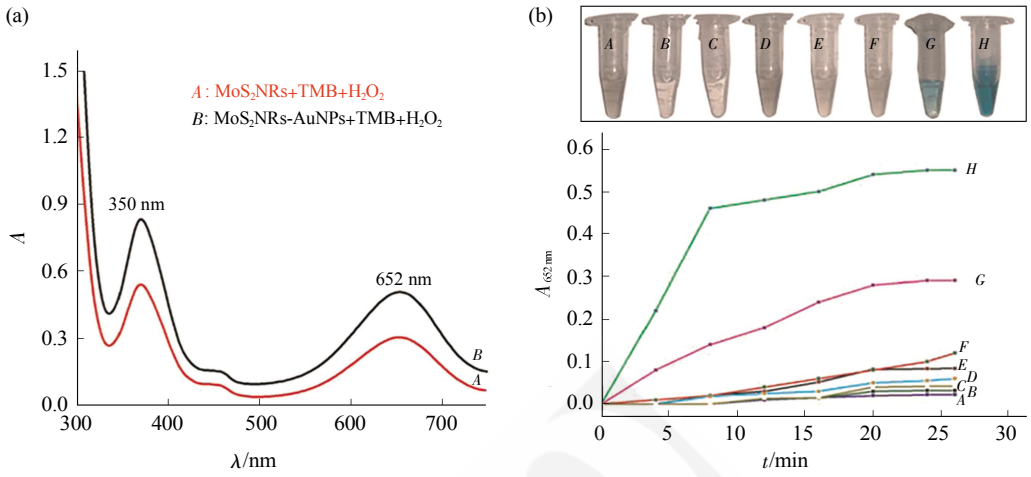

Fig. 27 Detection of cholesterol using MoS_2 NRs-Au NPs

(a) UV-*vis* spectrograph of different reaction systems. (b)Time-dependent absorbance changes at 652 nm of TMB in different reaction systems:(*A*)TMB, (*B*) H_2O_2+TMB, (*C*) MoS_2 NRs (*D*)MoS_2 NR+TMB, (*E*) MoS_2 NRs-Au NPs (*F*) MoS_2 NRs-AuNPs+TMB (*G*) TMB+MoS_2 NRs+H_2O_2 (*H*) TMB+MoS_2 NRs-AuNPs+H_2O_2[82].

and the synergistic interaction of two components. On this basis, they constructed a simple, sensitive and selective colorimetric assay to detect H_2O_2 and glucose in serum samples with or without visible light.

6 Conclusions and future perspectives

In summary, we give a brief overview in the progress of enzyme mimics based on 2D transition-metal dichalcogenide nanocomposites in recent years. This research field is still young and highly active, as indicated by the rapidly growing number of publications. There are still many rooms that can be taken into account for future research:

(1) Controllable synthesis of 2D transition-metal dichalcogenide nanocomposites with high-quality is still challenging.

(2) Another critical issue for 2D transition-metal dichalcogenide nanocomposite is how to maximize the interfacial contact between layered supports and nanoparticles.

(3) From an economic point of view, the design of novel 2D transition-metal dichalcogenide nanocomposites by reducing usage of Pt and remain high catalytic efficiencies is needed.

(4) Many reports on enzyme mimics with peroxidase-like activities, only a few other enzymatic systems have been studied, leaving a wide open space for future investigations.

(5) The design of multifunctional nanozymes based on two-dimentional transition-metal dichalcogenide for different applications, such as biosensors, nanocatalysts and nanomedicine is highly desirable.

In general, the enzyme mimic based on 2D transition-metal dichalcogenide nanocomposites and other graphene analogs of layered materials will thrive in near future.

References

[1] Gao L Z, Zhuang J, Nie L, *et al*. Intrinsic peroxidase-like activity of ferromagnetic nanoparticles. Nat Nanotechnol, 2007, **2**(9): 577−583

[2] Wei H, Wang E K. Nanomaterials with enzyme-like characteristics (nanozymes): next-generation artificial enzymes. Chem Soc Rev, 2013, **42**(14): 6060−6093

[3] Wang X H, Han Q S, Cai S F, *et al*. Excellent peroxidase mimicking property of CuO/Pt nanocomposites and their application as an ascorbic acid sensor. Analyst, 2017, **142** (13): 2500−2506

[4] Song Y, Qu K, Zhao C, *et al*. Graphene Oxide: Intrinsic peroxidase catalytic activity and its application to glucose detection. Adv Mater, 2010, **22**(19): 2206−2210

[5] Song Y J, Wang X H, Zhao C, *et al*. Label-free colorimetric detection of single nucleotide polymorphism by using single-walled carbon nanotube intrinsic peroxidase-like activity. Chem Eur J, 2010, **16**(12): 3617−3621

[6] Asati A, Santra S, Kaittanis C, *et al*. Oxidase-like activity of polymer-coated cerium oxide nanoparticles. Angew Chem, Int Ed, 2009, **48**(13): 2308−2312

[7] Pirmohamed T, Dowding J M, Singh S, *et al*. Nanoceria exhibit

redox state-dependent catalase mimetic activity. Chem Commun, 2010, **46**(16): 2736-2738

[8] Natalio F, Andre R, Hartog A F, *et al*. Vanadium pentoxide nanoparticles mimic vanadium haloperoxidases and thwart biofilm formation. Nat Nanotechnol, 2012, **7**(8): 530-535

[9] Comotti M, Della P C, Matarrese R, *et al*. The catalytic activity of "naked" gold particles. Angew Chem, Int Ed, 2004, **43** (43): 5812-5815

[10] Luo W, Zhu C, Su, S, *et al*. Self- catalyzed, self-limiting growth of glucose oxidase- mimicking gold nanoparticles. ACS Nano, 2010, **4**(12): 7451-7458

[11] Zheng X, Liu Q, Jing C, *et al*. Catalytic gold nanoparticles for nanoplasmonic detection of DNA hybridization. Angew Chem, Int Ed, 2011, **50**(50): 11994-11998

[12] Cai S F, Qi C, Li Y D, *et al*. PtCo bimetallic nanoparticles with high oxidaselike catalytic activity and their applications for magnetic-enhanced colorimetric biosensing. J Mater Chem B, 2016, **4**(10): 1869-1877

[13] Cai S F, Jia X H , Han Q S, *et al*. Porous PtAg nanoparticles with excellent multifunctional enzyme mimic activities and antibacterial effects. Nano Research, 2017, **10**(6): 2056-2069

[14] He H, Xu X , Wu H, *et al*. Enzymatic plasmonic engineering of Ag/Au bimetallic nanoshells and their use for sensitive optical glucose sensing. Adv Mater, 2012, **24**(13): 1736-1740

[15] Li L H, Wu Y, Lu J, *et al*. Synthesis of Pt-Ni/graphene *via in situ* reduction and its enhanced catalyst activity for methanol oxidation. Chem Commun, 2013, **49**(68): 7486-7488

[16] Zhao J, Hu W B, Li H Q, *et al*. One-step green synthesis of a ruthenium/graphene composite as a highly efficient catalyst. RSC Adv, 2015, **5**(10): 7679-7686

[17] Shearer C J, Cherevan A, Eder D. Application and future challenges of functional nanocarbon hybrids. Adv Mater, 2014, **26** (15): 2295-2318

[18] Hou Y, Wen Z H, Cui S M, *et al*. An advanced nitrogen-doped graphene/cobalt-embedded porous carbon polyhedron hybrid for efficient catalysis of oxygen reduction and water splitting. Adv Funct Mater, 2015, **25**(6): 872-882

[19] Guo Y J, Deng L, Li J, *et al*. Hemin-graphene hybrid nanosheets with intrinsic peroxidase- like activity for label-free colorimetric detection of single-nucleotide polymorphism. ACS Nano, 2011, **5**(2): 1282-1290

[20] Song Y J, Chen Y, Feng L Y, *et al*. Selective and quantitative cancer cell detection using target-directed functionalized graphene and its synergetic peroxidase-like activity. Chem Commun, 2011, **47**(15): 4436-4438

[21] Zuo X L, Peng C, Huang Q, *et al*. Design of a carbon nanotube/magnetic nanoparticle-based peroxidase- like nanocomplex and its application for highly efficient catalytic oxidation of phenols. Nano Res, 2009, **2**(8): 617-623

[22] Dong Y L, Zhang H G, Rahman Z U, *et al*. Graphene oxide-Fe_3O_4 magnetic nanocomposites with peroxidase-like activity for colorimetric detection of glucose. Nanoscale, 2012, **4** (13): 3969-3976

[23] Zhang L N, Deng H H, Lin F L, *et al*. *In situ* growth of porous platinum nanoparticles on graphene oxide for colorimetric detection of cancer cells. Anal Chem, 2014, **86**(5): 2711-2718

[24] Tao Y, Lin Y H, Huang Z Z, *et al*. Incorporating graphene oxide and gold nanoclusters: a synergistic catalyst with surprisingly high peroxidase-like activity over a broad pH range and its application for cancer cell detection. Adv Mater, 2013, **25**(18): 2594-2599

[25] Wang Q H, Kalantar-Zadeh K, Kis A, *et al*. Electronics and optoelectronics of two-dimensional transition metal dichalcogenides. Nat Nanotechnol, 2012, **7**(11): 699-712

[26] Chhowalla M, Shin H S, Eda G, *et al*. The chemistry of two-dimensional layered transition metal dichalcogenide nanosheets. Nat Chem, 2013, **5**(4): 263-275

[27] Mak K F, Lee C, Hone J, *et al*. Atomically thin MoS_2: a new direct-gap semiconductor. Phys Rev Lett, 2010, **105** (13): 136805_1-4

[28] Coleman J N, Lotya M, O'Neill A, *et al*. Two-dimensional nanosheets produced by liquid exfoliation of layered materials. Science, 2011, **331**(6017): 568-571

[29] Bogaert K, Liu S, Chesin J, *et al*. Diffusion-mediated synthesis of MoS_2/WS_2 lateral heterostructures. Nano Lett, 2016, **16** (8): 5129-5134

[30] Zeng H, Dai J, Yao W. *et al*. Valley polarization in MoS_2 monolayers by optical pumping. Nature Nanotech, 2012, **7** (8): 490-493

[31] Xie J, Zhang J, Li S, *et al*. Controllable disorder engineering in oxygen-incorporated MoS_2 ultrathin nanosheets for efficient hydrogen evolution. J Am Chem Soc, 2013, **135**(47): 17881-17888

[32] Du G, Guo Z, Wang S, *et al*. Superior stability and high capacity of restacked molybdenum disulfide as anode material for lithium ion batteries. Chem Commun, 2010, **46**(7): 1106-1108

[33] Lin T R, Zhong L S, Guo L Q, *et al*. Seeing diabetes: visual detection of glucose based on the intrinsic peroxidase-like activity of MoS_2 nanosheets. Nanoscale, 2014, **6**(20): 11856-11862

[34] Guo X R, Wang Y, Wu F Y, *et al*. A colorimetric method of analysis for trace amounts of hydrogen peroxide with the use of the nano-properties of molybdenum disulfide. Analyst, 2015, **140** (4): 1119-1126

[35] Li B L, Luo H Q, Lei J L, *et al*. Hemin-functionalized MoS_2 nanosheets: enhanced peroxidase-like catalytic activity with a steady state in aqueous solution. RSC Adv, 2014, **4** (46): 24256-24262

[36] Cai S, Han Q, Qi C, *et al*. $Pt_{74}Ag_{26}$ nanoparticle-decorated monolayer MoS_2 nanosheets as novel peroxidase mimics for highly selective colorimetric detection of H_2O_2 and glucose. Nanoscale, 2016, **8**(6): 3685-3693

[37] Qi C, Cai S, Wang X, *et al*. Enhanced oxidase/peroxidase-like activities of aptamer conjugated MoS_2/PtCu nanocomposites and their biosensing application. RSC Advances, 2016, **6** (60): 54949-54955

[38] Cai S, Han Q, Qi C, *et al*. MoS_2-Pt_3Au hybrids with enhanced peroxidase-like activities for selective colorimetric detection of phenol. Chin J Chem, 2017, **35**(5): 605-612

[39] Radisavljevic B, Radenovic A, Brivio J, *et al*. Single-layer MoS_2 transistors. Nat Nanotechnol, 2011, **6**(3): 147-150

[40] Sangwan V K, Arnold H N, Jariwala D, *et al*. Low-frequency electronic noise in single-layer MoS_2 transistors. Nano Lett, 2013, **13**(9): 4351-4355

[41] Zeng Z Y, Yin Z Y, Huang X, *et al*. Single-layer semiconducting nanosheets: high-yield preparation and device fabrication. Angew Chem, Int Ed, 2011, **50**(47): 11093-11097

[42] Yang L C, Wang S N, Mao J J, *et al*. Hierarchical MoS_2/Polyaniline Nanowires with excellent electrochemical performance for lithium-ion batteries. Adv Mater, 2013, **25**(8): 180−1184

[43] Jia T T, Kolpin A, Ma C S, *et al*. A graphene dispersed CdS-MoS_2 nanocrystal ensemble for cooperative photocatalytic hydrogen production from water. Chem Commun, 2014, **50**(10): 1185−1188

[44] Xiang Q J, Yu J G, Jaroniec M. Synergetic effect of MoS_2 and graphene as cocatalysts for enhanced photocatalytic H_2 production activity of TiO_2 nanoparticles. J Am Chem Soc, 2012, **134** (15): 6575−6578

[45] Chang K, Chen W. *In situ* synthesis of MoS_2/graphene nanosheet composites with extraordinarily high electrochemical performance for lithium ion batteries. Chem Commun, 2011, **47**(14): 4252−4254

[46] Han Q S, Wang X H, Jia X H, *et al*. CpG loaded MoS_2 nanosheets as multifunctional agents for photothermal enhanced cancer immunotherapy. Nanoscale, 2017, **9**(18): 5927−5934

[47] Han Q S, Cai S F, Yang L, *et al*. Molybdenum disulfide nanoparticles as multifunctional inhibitors against Alzheimer's disease. ACS Appl Mater. Interface, 2017, **9**(25): 21116−21123

[48] Lin T, Zhong L, Song Z, *et al*. Visual detection of blood glucose based on peroxidase-like activity of WS_2 nanosheets. Biosens Bioelectron, 2014, **62**(5): 302−307

[49] Zhao H, Li Y, Tan B, *et al*. PEGylated molybdenum dichalcogenides (PEG-MoS_2) nanosheets with enhanced peroxidase-like activity for colorimetric detection of H_2O_2. New J Chem, 2017, **41**(14): 6700−6708

[50] Zhou X, Wan L J, Guo Y G. Synthesis of MoS_2 nanosheet-graphene nanosheet hybrid materials for stable lithium storage. Chem Commun, 2013, **49**(18): 1838−1840

[51] Li B L, Luo H Q, Lei J L, *et al*. Hemin-functionalized MoS_2 nanosheets: enhanced peroxidase- like catalytic activity with a steady state in aqueous solution. RSC Adv, 2014, **4** (46): 24256−24262

[52] Adams B D, Wu G, Nigro S, Facile Synthesis of Pd －Cd nanostructures with high capacity for hydrogen storage. J Am Chem Soc, 2009, **131**(20): 6930−6931

[53] Cui C H, Li H H, Liu X J, *et al*. Surface composition and lattice ordering-controlled activity and durability of CuPt electrocatalysts for oxygen reduction reaction. ACS Catal, 2012, **2**(2): 916−924

[54] Ge S, Liu F, Liu W, *et al*. Colorimetric assay of K-562 cells based on folic acid-conjugated porous bimetallic Pd@Au nanoparticles for point-of-care testing. Chem Commun, 2014, **50**(4): 75−477

[55] Chen X, Su B, Cai Z, *et al*. PtPd nanodendrites supported on graphene nanosheets: A peroxidase-like catalyst for colorimetric detection of H_2O_2. Sensors and Actuators B, 2014, **201**(4): 286−292

[56] Zhao Y, Ye C, Liu W, *et al*. Tuning the composition of AuPt bimetallic nanoparticles for antibacterial application. Angew Chem Int Ed, 2014, **53**(31): 8127−8131

[57] Liu Y, Li D, Sun S. Pt-based composite nanoparticles for magnetic, catalytic, and biomedical applications. J Mater Chem, 2011, **21**(34): 12579−12587

[58] Choi S, Lee S U, Kim W Y, *et al*. Composition-controlled PtCo alloy nanocubes with tuned electrocatalytic activity for oxygen reduction. ACS Appl Mater Interfaces, 2012, **4**(11): 6228−6234

[59] Yin S, Li Z, Cheng L, *et al*. Magnetic PEGylated Pt_3Co nanoparticles as a novel MR contrast agent: *in vivo* MR imaging and long-term toxicity study. Nanoscale, 2013, **5**(24): 12464−12473

[60] Liu Z Y, Xin H L, Yu Z Q, *et al*. Atomic-scale compositional mapping and 3-dimensional electron microscopy of dealloyed PtCo3 catalyst nanoparticles with spongy multicore/shell structures. J Electrochem Soc, 2012, **159**(9): F554−F559

[61] Grass M E, Yue Y, Habas S E, *et al*. Silver ion mediated shape control of platinum nanoparticles: Removal of silver by selective etching leads to increased catalytic activity. J Phys Chem C, 2008, **112**(13): 4797−4804

[62] Zhang T, Lu Y, Luo G. Synthesis of hierarchical iron hydrogen phosphate crystal as a robust peroxidase mimic for stable H_2O_2 detection. ACS Appl Mater Interfaces, 2014, **6**(16): 14433−14438

[63] Wang G L, Xu X F, Qiu L, *et al*. Dual responsive enzyme mimicking activity of AgX nanoparticles and its application for cancer cell detection. ACS Appl Mater Interfaces, 2014, **6** (9): 6434−6442

[64] Pramanik A, Laha D, Pramanik P, *et al*. A novel drug “copper acetylacetonate” loaded in folic acid-tagged chitosan nanoparticle for efficient cancer cell targeting. J Drug Target, 2014, **22** (1): 23−33

[65] Galbiati A, Tabolacci C, Morozzo D R B, *et al*. Targeting tumor cells through chitosan-folate modified microcapsules loaded with camptothecin. Bioconjug Chem, 2011, **22**(6): 1066−1072

[66] Singh G, Kumar M, Soni U, *et al*. Cancer cell targeting using folic acid/anti-HER2 antibody conjugated fluorescent CdSe/CdS/ZnS-MPA and CdTe-MSA quantum dots. J Nanosci Nanotechnol, 2015, **15**(12): 9382−95

[67] Yang S, Chen J, Lin, F, *et al*. Colorectal cancer cell detection by folic acid-conjugated chitosan nanoparticles. Biomed Eng Appl Basis Commun, 2010, **22**(01): 9−17

[68] Ferreira C S M, Matthews C S, Missailidis S. DNA aptamers that bind to MUC1 tumour marker: design and characterization of MUC1-binding single-stranded DNA aptamers. Tumor Biol, 2006, **27**(6): 289−301

[69] Ferreira C S M, Cheung M C, Missailidis S, *et al*. Phototoxic aptamers selectively enter and kill epithelial cancer cells. Nucleic Acids Res, 2009, **37**(3): 866−876

[70] Liao G, Wang M, Ou Y. IGF-1-induced epithelial-mesenchymal transition in MCF-7 cells is mediated by MUC1. Cellular Signalling, 2014, **26**(10): 2131−2137

[71] Shen Q, Rahn J J, Zhang J, *et al*. MUC1 initiates Src-CrkL-Rac1/Cdc42-mediated actin cytoskeletal protrusive motility after ligating intercellular adhesion molecule. Mol Cancer Res, 2008, **6**(4): 555−567

[72] McGuckin M A, Walsh M D, Hohn B G, *et al*. Prognostic significance of MUC1 epithelial mucin expression in breast cancer. Hum Pathol, 1995, **26**(4): 432−439

[73] Wang L, Ma J, Liu F, *et al*. Expression of MUC1 in primary and metastatic human epithelial ovarian cancer and its therapeutic significance. Gynecol Oncol, 2007, **105**(3): 695−702

[74] Mahanta S, Fessler S P, Park J, *et al*. A minimal fragment of MUC1 mediates growth of cancer cells. PLoS One, 2008, **3**(4): e2054

[75] Hu Y, Duan J H, Zhan Q M, *et al*. Novel MUC1aptamer selectively delivers cytotoxic agent to cancer cells *in vitro*. PLoS One, 2012, **7**(2): e31970

[76] Wang X H, Han Q S, Yu N, *et al*. Aptamer-conjugated graphene oxide-gold nanocomposites for targeted chemo-photothermal therapy of cancer cells. J Mater Chem B, 2015, **3**(19): 4036−4042

[77] Ren L F, Marquardt M A, Lech J J, Estrogenic effects of nonylphenol on pS2, ER and MUC1 gene expression in human breast cancer cells-MCF-7. Chem Biol Interact, 1997, **104** (1): 55−64

[78] Croce M V, Colussi A G, Price M R, *et al*. Identification and characterization of different subpopulations in a human lung adenocarcinoma cell line (A549). Pathol Oncol Res, 1999, **5** (3): 197−204

[79] Zhou W, Yin Z, Du Y, *et al*. Synthesis of few-layer MoS_2 nanosheet-coated TiO_2 nanobelt heterostructures for enhanced photocatalytic activities. Small, 2013, **9**(1): 140−147

[80] Xu J, Zhao T, Liang Z, *et al*. Facile preparation of AuPt alloy nanoparticles from organometallic complex precursor. Chem Mater, 2008, **20**(5): 1688−1690

[81] Sun Z, Zhao QS, Zhang GH, *et al*. Exfoliated MoS_2 supported Au-Pd bimetallic nanoparticles with core-shell structures and superior peroxidase-like activities. RSC Adv, 2015, **5** (14): 10352−10357

[82] Nirala N R, Pandey S, Bansal A, *et al*. Different shades of cholesterol: Gold nanoparticles supported on MoS_2 nanoribbons for enhanced colorimetric sensing of free cholesterol. Biosens Bioelectron, 2015, **74**(6): 207−213

[83] Peng J, Weng J, Enhanced peroxidase-like activity of MoS_2/graphene oxide hybrid with light irradiation for glucose detection. Biosens. Bioelectron, 2017, **89**(1): 652−658

二维过渡金属硫化物纳米复合材料的模拟酶特性及应用 *

杨 蓉[1,2)**] 蔡双飞[1)] 王 琛[1,2)**]

([1)] 国家纳米科学中心，中国科学院纳米生物安全与生物医学重点实验室，中国科学院纳米卓越中心，北京 100190；
[2)] 中国科学院大学中丹学院，北京 100190)

摘要 纳米酶是一个非常令人兴奋和有希望的研究领域，旨在使用各种纳米材料模仿天然酶的一般原理，并在许多领域提供了大量实际应用．天然酶具有一些内在的缺点，如成本高、稳定性低、储存困难，以及催化活性对环境条件的敏感性．而纳米酶显示出低成本，高稳定性和高效活性．各种过氧化物酶和 / 或氧化酶模拟物已经取得了很大的进展．本综述介绍了关于二维过渡金属硫化物纳米复合材料的纳米酶特性的最新研究进展．

关键词 二维过渡金属硫化物，纳米复合材料，模拟酶，过氧化物酶，生物传感

学科分类号 Q811，Q814 **DOI**: 10.16476/j.pibb.2017.0470

* 国家重点研发计划(2016YFC0207102)，国家自然科学基金资助项目(21573050，21501034) 及中国科学院战略性科技先导项目(A 类)(XDA09030303)资助.

** 通讯联系人.

杨 蓉. Tel: 010-82545616, E-mail: yangr@nanoctr.cn

王 琛. Tel: 010-82545561, E-mail: wangch@nanoctr.cn

收稿日期：2017-12-18，接受日期：2018-01-20